PFC/JA-90-22

Guiding Center Stochasticity and Transport Induced by Electrostatic Waves

K. Kupfer, A. Bers, and A. K. Ram

June 1990

Plasma Fusion Center
Massachusetts Institute of Technology
Cambridge, MA 02139 USA

To Appear in : *Proceedings of the Topical Conference on Research Trends in Nonlinear and Relativistic Effects in Plasmas,* February 5-8, 1990, La Jolla, California.

Guiding Center Stochasticity and Transport

Induced by Electrostatic Waves

K. Kupfer, A. Bers, and A. K. Ram

TABLE OF CONTENTS

To appear in: Proceedings of the Topical Conference on Research Trends in Nonlinear and Relativistic Effects in Plasmas, February 5-8, 1990, La Jolla Institute, La Jolla, California.

Guiding Center Stochasticity and Transport Induced by Electrostatic Waves

K. Kupfer, A. Bers, and A.K. Ram

Plasma Fusion Center and Research Laboratory of Electronics
Massachusetts Institute of Technology
Cambridge, Massachusetts 02139

Abstract

We present a study of plasma transport driven by externally imposed wave fields; the transport arises from the induced chaotic particle dynamics. In particular, we examine the guiding center motion of charged particles interacting with electrostatic waves in a tokamak. This motion is described by a time-dependent Hamiltonian in a four-dimensional phase space composed of the guiding center's three position coordinates and its velocity along the magnetic field. As a specific focus, the work is applied to electrons in lower-hybrid current drive (LHCD) fields. We examine the dynamics for two cases: (i) a large ensemble of randomly phased waves, and (ii) a few large amplitude waves. For case (i), we calculate the local quasilinear diffusion tensor in the two-dimensional action space of the guiding center and compare it to numerical observations of the stochastic diffusion induced by the same spectrum of waves. An average radial diffusion coefficient is estimated from the quasilinear tensor and we discuss its scaling for typical LHCD parameters. In case (ii), we find enhanced radial transport in the presence of waves whose corresponding wave-particle resonance conditions are simultaneously satisfied at a single point in action space. In the vicinity of this point the radial excursions are not limited by the trapping width of the resonances. The mean square radial deviation of an orbit from its initial average flux surface, $\sigma(t)$, is found to obey a power law for long times, i.e. $\sigma(t) \approx \sigma_o t^\gamma$. When the amplitude of the waves is small enough that their primary resonances retain stable fixed points (even though the overlap criteria is satisfied), we find that γ is below unity, indicating an anomalous diffusive process; at larger amplitudes $\gamma \approx 1$. When the shear of the magnetic field lines is taken to be zero, resonances can coalesce throughout action space. In the presence of such a degenerate resonance we find that orbits will exhibit a "stochastic streaming" in the radial direction.

I Introduction

In this paper we are studying the guiding center motion of magnetically confined charged particles interacting with electrostatic waves in a plasma. As a specific focus, the work is applied towards describing the wave induced radial transport of electrons during lower-hybrid current drive (LHCD) in a tokamak. During LHCD, electrons interact with the wave field and experience stochastic accelerations along magnetic field lines. Radial transport follows because the toroidal ∇B and curvature drifts are coupled to the parallel stochastic acceleration. In addition, the perpendicular component of the wave field gives rise to a fluctuating $E \times B$ drift which also leads to radial transport. This intrinsic wave induced transport may be partially responsible for the observed anomalous confinement of superthermal electrons during LHCD [1]. It is also important to consider wave induced transport when attempting to control the wave induced current profile.

Guiding center motion is described by a time-dependent Hamiltonian in a four-dimensional phase space composed of the guiding center's three position coordinates and its parallel velocity (along the magnetic field). The stochastic motion of guiding centers through prescribed wave fields has been studied previously in two limiting cases: motion along the magnetic field with no drifts [2, 3, 4], and drift motion without parallel wave driven accelerations [5, 6]. In each of these cases one can view the dynamics in a two-dimensional surface of section and the relevant diffusive process is one-dimensional. In our recent work, the radial component of the guiding center drift was coupled to a stochastic two-dimensional map which determined the parallel motion [7]. We are generalizing these approaches by considering the dynamics in a four-dimensional phase space. We use Littlejohn's Lagrangian formulation of guiding center motion [8] to derive canonical coordinates for a tokamak equilibrium with an imposed electrostatic wave field. Using the standard approach of classical mechanics, we obtain the generating function which relates the toroidal coordinates to the action-angle coordinates of a particle's unperturbed orbit (the case when the imposed wave field vanishes). One can derive an explicit form for the action-angle coordinate transformation for circulating particles in a low β circular tokamak. This is done by expanding the generating function to exploit the fact that the deviation of an electron's orbit from its average flux surface is small compared to the scale length of the magnetic inhomogeneity. Upon transforming the wave field from toroidal coordinates to action-angle coordinates, it is written as a Fourier series in the angles and each component is associated with a discrete curve in action space along which

the wave-particle resonance condition is satisfied. Ignoring drift motion leads to the usual resonance overlap criterion for the formation of a thick stochastic layer in a two-dimensional phase space which describes the parallel motion. When the drift motion is included, the stochastic process leads to radial transport. Generically, wave-particle resonance curves will intersect at points in action space where the ratio of the unperturbed frequencies is a rational number (i.e. rational unperturbed KAM tori). We show that in the vicinity of these intersections, particles can make large excursions in the radial direction. This leads to enhanced diffusion in the presence of a few large amplitude waves. Conventional quasilinear treatments of transport in RF heated plasmas [9, 10] cannot account for such effects.

For LHCD, determining the wave field in the plasma from that launched at the edge is a complex problem which has not yet been solved. Here we assume that there exists in the core of the plasma some spectrum of electrostatic travelling waves which approximately satisfy the local dispersion relation for frequencies above the lower-hybrid frequency. We consider two examples. In the first example we calculate the quasilinear diffusion tensor in action space [11] for the case of a broad spectrum of randomly phased waves; we compare this to the diffusion observed by numerically following the exact, stochastic orbits. In the second example we consider the stochasticity and radial transport induced by a few large amplitude waves.

The paper is divided into six sections, organized in the following manner. Canonical coordinates for the guiding center are derived in Section II. In Section III an explicit form for the action-angle coordinate transformation is developed for circulating particles. In Section IV general features of the guiding center's interaction with the wave field are discussed. In Section V we consider quasi-linear diffusion induced by a broad spectrum of waves and in Section VI we consider the case of a few large amplitude waves. Our conclusions are in Section VII. In Appendix A we derive the canonical coordinates for a magnetized slab with shear. Appendix B contains the guiding center equations of motion in toroidal coordinates.

II Hamiltonian Guiding Center Formalism

Starting from the Lagrangian formulation of guiding center motion developed by Littlejohn [8], we will derive canonical coordinates for an axisymmetric, time-independent equilibrium under the effect of electrostatic waves. The Lagrangian is

$$L(\mathbf{x},\dot{\mathbf{x}},u,\dot{u}) = [\frac{e}{m}\mathbf{A}(\mathbf{x}) + u\mathbf{b}(\mathbf{x})]\cdot\dot{\mathbf{x}} - H(u,\mathbf{x},t) \quad , \tag{1}$$

where

$$H = \frac{1}{2}u^2 + MB(\mathbf{x}) + \frac{e}{m}\Phi(\mathbf{x},t) \quad , \tag{2}$$

$\mathbf{x}$ is the three-dimensional spatial position vector of the guiding center, u is its parallel velocity, and M is its magnetic moment divided by its mass. The vector potential is $\mathbf{A}(\mathbf{x})$, $\mathbf{B}(\mathbf{x})$ is the magnetic field, and $\Phi(\mathbf{x},t)$ is the scalar potential of the electrostatic wave-field. Also $\mathbf{b}(\mathbf{x}) = \mathbf{B}/B$ and $B(\mathbf{x}) = |\mathbf{B}|$. If we let z_i denote one of the four guiding center coordinates, $\mathbf{x}$ and u, then the guiding center's motion is determined by the four Euler-Lagrange equations,

$$\frac{d}{dt}\frac{\partial L}{\partial \dot{z}_i} = \frac{\partial L}{\partial z_i} \quad . \tag{3}$$

Since L is independent of $\dot{u}$, one finds that $\partial L/\partial u = 0$, so that u is in fact the parallel velocity, i.e. $u = \mathbf{b}\cdot\dot{\mathbf{x}}$. The remaining three Euler-Lagrange equations determine the perpendicular guiding center drift and the parallel acceleration. With a little algebra one obtains the following equations of motion:

$$\dot{\mathbf{x}} = (B_{||}^{\star})^{-1}[u\mathbf{B}^{\star} + \mathbf{b}\times(\frac{m}{e}M\nabla B + \nabla\Phi)] \quad , \tag{4}$$

$$\dot{u} = -\frac{\mathbf{B}^{\star}}{B_{||}^{\star}}\cdot(\frac{e}{m}\nabla\Phi + M\nabla B) \quad , \tag{5}$$

where $\mathbf{B}^{\star} = \mathbf{B} + (mu/e)\nabla\times\mathbf{b}$ and $B_{||}^{\star} = \mathbf{b}\cdot\mathbf{B}^{\star}$. Since the magnetic moment is conserved, we consider it a parameter and not a dynamical variable. This restricts us to the case when the frequency of the wave field is much smaller than the gyro-frequency of the particles under consideration, a condition which is well satisfied by electrons in LHCD fields. It is assumed that the electron Larmor radius is small compared to the perpendicular wavelength of the electrostatic field. The amplitude of the wave field is restricted by the usual limitations of guiding center analysis, which require both the parallel acceleration and the $E\times B$ drift during a gyro-period to be small in the following sense: $|k_{||}^2\Phi/(\omega_{rf}B)| \ll 1$

and $|mk_\perp^2\Phi/(eB^2)| \ll 1$, where $k_\parallel$ and $k_\perp$ are characteristic parallel and perpendicular wave numbers and ω_{rf} is the frequency of the wave field ($\omega_{rf} = 2\pi f_{rf}$).

We now transform the Lagrangian into the toroidal coordinates (ψ, θ, ϕ), where ψ is the usual poloidal flux function and ϕ is the toroidal angle. The coordinate θ is chosen so that $\nabla\theta$ is perpendicular to both $\nabla\psi$ and $\nabla\phi$. Also θ increases by 2π upon one rotation around a flux surface at fixed toroidal angle. Using these coordinates the magnetic field for a scalar pressure MHD equilibrium can be written as [12]

$$\mathbf{B} = g(\psi)\nabla\phi + F(\psi,\theta)\nabla\theta \quad , \tag{6}$$

where the vector potential is chosen to be

$$\mathbf{A} = \psi\nabla\phi - G(\psi,\theta)\nabla\theta \quad . \tag{7}$$

These relations define the functions $g(\psi)$, $F(\psi,\theta)$, and $G(\psi,\theta)$. It is straightforward to show that the θ average of $\partial G(\psi,\theta)/\partial\psi$ is the tokamak safety factor $q(\psi)$ [13]. Substituting (6) and (7) into (1) the Lagrangian becomes

$$L = p_\phi\dot{\phi} + p_\theta\dot{\theta} - H \quad , \tag{8}$$

where the momenta conjugate to ϕ and θ are

$$p_\phi = \psi + g(\psi)u/B \quad , \tag{9}$$

and

$$p_\theta = -G(\psi,\theta) + F(\psi,\theta)u/B \quad . \tag{10}$$

The system has been normalized in the following manner: the units of velocity are v_o (chosen to make the parallel velocity of order unity, i.e. $v_o \sim \omega_{rf}/k_\parallel$) and the units of time are R_o/v_o, where R_o is the major radius. The normalized Hamiltonian is

$$H = u^2/2 + MB(\psi,\theta) + \Phi(\psi,\theta,\phi,t) \quad , \tag{11}$$

where the electrostatic potential is normalized to mv_o^2/e and the magnetic field is normalized to B_o (the toroidal field on axis). The constant M is now the magnetic moment of the guiding center normalized to mv_o^2/B_o. Both ψ and G are normalized to mR_ov_o/e, whereas F and g are normalized to R_oB_o. It is convenient to introduce the function $G'(\psi,\theta) \equiv \partial G(\psi,\theta)/\partial\psi$. With the above normalization the functions $g(\psi)$, $F(\psi,\theta)$, $B(\psi,\theta)$, and $G'(\psi,\theta)$ are all

slowly varying in ψ. Generally one cannot invert (9) and (10) to obtain ψ and u as explicit functions of the canonical momenta. It is easy, however, to obtain the equations of motion in the coordinates $(\rho_{\|}, \psi, \theta, \phi)$, where $\rho_{\|} \equiv u/B$. The results are shown in Appendix B. The formalism is most similar to that of White [14] except that we have used an orthogonal coordinate system to describe the tokamak geometry. In general, these results differ from those obtained by Kaufman [11] because the parallel velocity in our formulation is not strictly proportional to the time rate of change of the toroidal angle (as is the case when the guiding center is following a magnetic field line).

In the absence of the electrostatic potential, the toroidal angular momentum, p_ϕ, and the unperturbed Hamiltonian, H_o, are both conserved. (Note, $H_o = u^2/2 + MB(\psi, \theta)$.) Transforming to the action-angle coordinates of the unperturbed Hamiltonian is done by following the standard procedure of classical mechanics [15]. The definitions of H_o and p_ϕ are used to obtain p_θ as a function of θ, H_o, and p_ϕ. The poloidal action, I_θ, is defined as the area (divided by 2π) in the (p_θ, θ) plane enclosed by, or beneath a curve of constant H_o and p_ϕ, depending on whether the orbit is trapped, or circulating. This is written as

$$I_\theta = \oint \frac{d\theta}{2\pi} p_\theta(\theta; H_o, p_\phi) \quad . \tag{12}$$

The toroidal action, I_ϕ, is identical to p_ϕ. The canonically conjugate angle variables, ζ_θ and ζ_ϕ, are obtained from the generating function,

$$S(\theta, \phi, I_\theta, I_\phi) = \int^\theta d\theta' p_\theta(\theta'; H_o(I_\theta, I_\phi), I_\phi) + I_\phi \phi \quad , \tag{13}$$

by differentiating with respect to the actions,

$$\zeta_i = \frac{\partial S}{\partial I_i} \quad , \tag{14}$$

where the subscript i denotes either θ, or ϕ. Also, the identities, $p_\theta = \partial S/\partial\theta$ and $p_\phi = \partial S/\partial\phi$, are recovered from the generating function. Note, that H_o is a function of the actions as given implicitly by (12). The unperturbed frequencies for both the θ and ϕ motions are

$$\dot{\zeta}_i = \frac{\partial H_o}{\partial I_i} \equiv \Omega_i(I_\theta, I_\phi) \quad . \tag{15}$$

Physically, Ω_θ, is the bounce (transit) frequency of a trapped (circulating) particle. Ω_ϕ is the bounce-average of $\dot{\phi}$, which is equivalent to $\Omega_\theta \Delta\phi/2\pi$, where $\Delta\phi$ is the amount of toroidal rotation during one poloidal orbit. In action-angle coordinates the Hamiltonian takes on the form

$$H = H_o(\mathbf{I}) + \Phi(\mathbf{I}, \boldsymbol{\zeta}, t) \quad , \tag{16}$$

where $\mathbf{I} = (I_\theta, I_\phi)$ and $\boldsymbol{\zeta} = (\zeta_\theta, \zeta_\phi)$.

III Action-Angle Coordinates For Circulating Electrons

In this section we consider an ensemble of electrons in the vicinity of a specific flux surface in the core of the plasma. Furthermore, we consider only circulating electrons since they are primarily responsible for the absorption of the RF power during LHCD. We write the functions $g(\psi)$, $F(\psi,\theta)$, $B(\psi,\theta)$, and $G'(\psi,\theta)$ as power series in the inverse aspect ratio, ϵ, defined as r/R_o, where r is the radial distance from the magnetic axis:

$$\begin{aligned} g(\psi) &= 1+\mathcal{O}\epsilon^2 \\ F(\psi,\theta) &= \mathcal{O}\epsilon^2 \\ B(\psi,\theta) &= 1-\epsilon(\psi)\cos\theta+\mathcal{O}\epsilon^2 \\ G'(\psi,\theta) &= q(\psi)+q_1\cos\theta+\mathcal{O}\epsilon^2 \quad . \end{aligned} \tag{17}$$

The ordering in (17) assumes a low β circular equilibrium [13] and reflects the fact that the ratio of the poloidal to toroidal field is of order ϵ and modifications to the vacuum toroidal field are of order ϵ^2. The safety factor $q(\psi)$ is the poloidal average of $G'(\psi,\theta)$ and $q_1(\psi)$ is of order ϵ, as needed to satisfy the identity $G' = (\mathbf{B}\cdot\nabla\phi)/(\mathbf{B}\cdot\nabla\theta)$. For example, if one ignores the Shafranov shift of the flux surfaces, so that $\psi = \psi(r)$, then $q_1(\psi) = -\epsilon(\psi)q(\psi)$. In a self consistent toroidal equilibrium the shift of the surfaces must be included to correctly determine $q_1(\psi)$ through order ϵ. We ignore all terms of order ϵ^2 and higher.

To obtain an explicit form for the action-angle transformation we exploit the fact that both $B(\psi,\theta)$ and $G'(\psi,\theta)$ are slowly varying functions of ψ; i.e $B = B(\lambda\psi,\theta)$ and $G' = G'(\lambda\psi,\theta)$, where $\lambda \ll 1$. Physically, the size of λ is obtained by considering the relation between radial distance and the normalized poloidal flux, $\Delta r = \rho_\theta \Delta\psi$, where $\rho_\theta = mv_o/eB_\theta$ and B_θ is the poloidal component of the magnetic field at $r = r_o$. Typically ρ_θ is small compared to the radial distance over which B and G' vary. We now consider a two parameter expansion, in which both ϵ and λ are small. We consider λ to be of order ϵ, so that we keep terms of first order in λ, while ignoring terms of order $\epsilon\lambda$ and λ^2. For fast electrons in the core of the plasma, $\lambda \sim \rho_\theta/r_o \sim 10^{-2}$, whereas $\epsilon_o \sim 10^{-1}$. Technically our expansion should go to second order in ϵ to consistently retain terms of first order in λ. However, we shall see that going to first order in λ allows us to treat the important physical effect of magnetic shear; going to second order in ϵ would make things unnecessarily complicated. By ignoring terms of order $\epsilon\lambda$, we take $\epsilon(\psi) \approx \epsilon_o$ and $q_1(\psi) \approx q_{1o}$, where the subscript denotes that each

quantity is evaluated at the surface r_o. The safety factor is of order unity so we expand it to first order in λ, i.e.

$$q(\psi) \approx q_o + q_o s_o \psi \quad , \tag{18}$$

where s_o is of order λ and represents the shear of the magnetic field. Note that we have chosen $\psi = 0$ at $r = r_o$. Using these expansions in (9) and (10) yields the canonical momenta,

$$p_\phi = \psi + u(1 + \epsilon_o \cos\theta) \tag{19}$$

$$\begin{aligned} p_\theta &= -\int^{\psi} d\psi' G'(\psi', \theta) \\ &= -q_o(\psi + \frac{s_o}{2}\psi^2) - q_{1o}\psi \cos\theta \quad . \end{aligned} \tag{20}$$

To the same order the unperturbed Hamiltonian is $H_o = u^2/2 - M\epsilon_o \cos\theta$, where we have dropped the additive constant, M. For well circulating particles, which satisfy M/H_o of order unity or smaller, one obtains the following relations for $u(\theta, H_o)$ and $\psi(\theta, H_o, p_\phi)$:

$$u \approx \hat{u} + (M\epsilon_o/\hat{u})\cos\theta \quad , \tag{21}$$

$$\psi \approx \hat{\psi} - \epsilon_o(\hat{u} + M/\hat{u})\cos\theta \quad , \tag{22}$$

where $\hat{u} \equiv \sqrt{2H_o}$ and $\hat{\psi} \equiv p_\phi - \hat{u}$. The poloidal action is obtained by substituting (22) into (20) and averaging in θ; ignoring terms of order ϵ^2 and $\epsilon\lambda$ one finds that

$$I_\theta \approx -q_o\hat{\psi} - \frac{q_o s_o}{2}\hat{\psi}^2 \quad . \tag{23}$$

Noting that $p_\phi = I_\phi$, we can write the unperturbed Hamiltonian as

$$H_o = \hat{u}^2/2 = (1/2)[I_\phi - \hat{\psi}(I_\theta)]^2 \quad . \tag{24}$$

From H_o it follows that $\Omega_\phi = \hat{u} = q(\hat{\psi})\Omega_\theta$; ignoring terms of first order in λ would result in $q(\hat{\psi}) \approx q_o$, so that the ratio of the unperturbed frequencies would be a constant. The generating function in (13) can now be written explicitly to the required order

$$S(\theta, \phi, I_\theta, I_\phi) = I_\theta\theta + I_\phi\phi + \epsilon_o S_T(I_\theta, I_\phi)\sin\theta \quad , \tag{25}$$

where

$$S_T = q_o I_\phi + (1 + \frac{q_{1o}}{q_o\epsilon_o})I_\theta + \frac{q_o^2 M}{(q_o I_\phi + I_\theta)} \quad . \tag{26}$$

One obtains $\zeta_\theta = \theta + \epsilon_o(\partial S_T/\partial I_\theta)\sin\theta$ which is easily inverted through first order in ϵ to obtain $\theta \approx \zeta_\theta - \epsilon_o(\partial S_T/\partial I_\theta)\sin\zeta_\theta$. Similarly one obtains the relation $\phi \approx \zeta_\phi - \epsilon_o(\partial S_T/\partial I_\phi)\sin\zeta_\theta$. We thus have the following transformation equations:

$$\theta \approx \zeta_\theta - [1 + \frac{q_{1o}}{q_o\epsilon_o} - \frac{q_o^2 M}{(q_o I_\phi + I_\theta)^2}]\epsilon_o \sin\zeta_\theta \tag{27}$$

$$\phi \approx \zeta_\phi - [q_o - \frac{q_o^3 M}{(q_o I_\phi + I_\theta)^2}]\epsilon_o \sin\zeta_\theta \tag{28}$$

$$\psi \approx \hat{\psi}(I_\theta) - [I_\phi + \frac{I_\theta}{q_o} + \frac{q_o M}{(q_o I_\phi + I_\theta)}]\epsilon_o \cos\zeta_\theta \quad . \tag{29}$$

The equation for ψ was obtained by substituting ζ_θ for θ in the order ϵ term of (22). Using these equations, the electrostatic potential can be transformed from the toroidal coordinates, ψ, θ, and ϕ, to action-angle coordinates.

Let us briefly discuss the physics of various terms that arise in the above transformation. The order ϵ terms signify the toroidal effects, the parallel magnetic gradient and the curvature of the field lines. These give rise to oscillations in both $\theta(t)$ and $\phi(t)$, as well as in the radial coordinate $\psi(t)$, the latter coming from the combination of the ∇B and curvature drifts. The order ϵ oscillation in ϕ vanishes when $M \approx I_\phi + I_\theta/q_o$, in which case the oscillation along the field line from the magnetic mirror is just cancelled by the shrinking of the pathlength as the particle rotates from the outside to the inside of the tokamak. For fast electrons during LHCD the curvature effects will dominate since M will typically be much smaller than the average parallel energy, H_o. The only order λ contribution comes from the shear of the magnetic field lines, i.e. q is not a constant so that the proportionality between Ω_θ and Ω_ϕ depends on the poloidal action. We note that the order $\epsilon\lambda$ terms, which have been neglected here, would be needed to properly treat trapped particles since it is these terms that give rise to the toroidal precession of the banana orbit.

IV Stochasticity In Action-Angle Coordinates

During LHCD the RF wave-field is driven at a single frequency, ω, by a source at the edge of the plasma. We write the potential as $\Phi = \mathrm{Re}\{\Phi_c(\psi,\theta,\phi)e^{-i\omega t}\}$, where Φ_c is a complex function of the original toroidal coordinates. The electron dynamics is obtained by transforming Φ_c into the above action-angle coordinates. Since the transformed potential is a periodic function of the angles, ζ_θ and ζ_ϕ, we can write it as the following Fourier series:

$$\Phi = \mathrm{Re}\{\sum_{n,l} C_{n,l}(\mathbf{I})e^{i(n\zeta_\phi + l\zeta_\theta - \omega t)}\} \quad , \tag{30}$$

where $C_{n,l}(\mathbf{I})$ is a complex function of the actions. We represent the transformation to action-angle coordinates as follows:

$$\phi = \zeta_\phi + \Lambda(\zeta_\theta, \mathbf{I}) \tag{31}$$

$$\theta = \Theta(\zeta_\theta, \mathbf{I}) \tag{32}$$

$$\psi = \Psi(\zeta_\theta, \mathbf{I}) \quad , \tag{33}$$

where explicit forms for Λ, Θ, and Ψ can be obtained by direct comparison with equations (27)-(29). The Fourier coefficients are

$$C_{n,l}(\mathbf{I}) = \int \frac{d\zeta_\theta}{2\pi} e^{-il\zeta_\theta + in\Lambda(\zeta_\theta, \mathbf{I})} \Phi_n(\Theta(\zeta_\theta, \mathbf{I}), \Psi(\zeta_\theta, \mathbf{I})) \quad , \tag{34}$$

where

$$\Phi_n(\theta, \psi) = \int \frac{d\phi}{2\pi} e^{-in\phi} \Phi_c(\theta, \psi, \phi) \quad . \tag{35}$$

The wave-particle resonance condition is simply $n\Omega_\phi(\mathbf{I}) + l\Omega_\theta(\mathbf{I}) = \omega$, which defines a curve in the two-dimensional action space. For a single mode (i.e. a distinct n and l) the actions will no longer be conserved, but there will still exist two independent constants of motion. These are easily found to be $nI_\theta - lI_\phi$, $\omega I_\phi - nH$, and $\omega I_\theta - lH$, where two of the three are independent (note H is the complete Hamiltonian). The orbits in this case are regular everywhere in phase space. For two modes it is easily shown that there will be only one constant of motion, in which case the dynamics can be obtained from an autonomous Hamiltonian with two degrees of freedom. Generally, there will be three or more modes and no constants of motion. In this case there exists three types of motion[16]: regular motion on a KAM torus, stochastic motion across resonances in the region where they overlap, and stochastic motion along resonances which are interconnected in action space (i.e. Arnold diffusion).

Physically the unperturbed guiding center motion has two well distinguished time scales, fast motion in the parallel direction (along the magnetic field) and slow drifts across the field. In the case of LHCD, the basic mechanism for induced stochastic dynamics arises from parallel accelerations caused by the waves. Ignoring the drift motion altogether will lead to the usual resonance overlap criterion for the formation of a thick stochastic layer in a two dimensional phase plane which describes the parallel motion alone. On a slower time scale this is coupled to the drift motion enabling particles to shift their average radial position. After a long time, particles can make large excursions perpendicular to the magnetic field, which in turn effects a gradual change in the structure of their parallel dynamics. For example, KAM curves in the parallel portion of phase space will gradually shift allowing particles to move from one resonance to another, even when such a transition is prohibited by motion in the parallel phase plane alone. The latter effect is Arnold diffusion.

To separate the fast motion along the magnetic field from the slow perpendicular motion, we introduce the following linear transformation of the action-angle coordinates:

$$\begin{aligned} I_\phi &= p_1 + p_2 \\ I_\theta &= -q_o p_2 \\ z_1 &= \zeta_\phi \\ z_2 &= \zeta_\phi - q_o \zeta_\theta \quad . \end{aligned} \tag{36}$$

The new coordinates are z_1 and z_2, and their respective canonical momenta are p_1 and p_2. Note, the generating function for this transformation is $S(\boldsymbol{\zeta}, \mathbf{p}) = (p_1 + p_2)\zeta_\phi - q_o p_2 \zeta_\theta$. Using equation (24) and (23) and neglecting terms of order s_o^2 (since s_o is of order λ), one can write the Hamiltonian as

$$H = \frac{p_1^2}{2} + s_o p_1 \frac{p_2^2}{2} + \Phi(\mathbf{p}, \mathbf{z}, t) \quad . \tag{37}$$

Following from (30) the potential is

$$\Phi = \mathrm{Re}\{\sum_{\mathbf{k}} C_{\mathbf{k}}(\mathbf{p}) e^{i(k_1 z_1 + k_2 z_2 - \omega t)}\} \quad , \tag{38}$$

where $k_1 = n + l/q_o$, $k_2 = -l/q_o$, $\mathbf{k} = (k_1, k_2)$, and $C_{\mathbf{k}}(\mathbf{p}) = C_{n,l}(\mathbf{I})$. If we take q_o to be a rational value then Φ is periodic in both z_1 and z_2 (the periodicity length for z_1 is an integer multiple of 2π depending on q_o, and for z_2 it is $2\pi q_o$). In Appendix A we derive this Hamiltonian for a magnetized slab with shear; the difference between a slab and a torus is contained in the coefficients $C_{\mathbf{k}}(\mathbf{p})$ of the wave spectrum, which are determined by equation (34) for a torus. From the Hamiltonian (37), we define the unperturbed frequencies $\boldsymbol{\Omega}(\mathbf{p}) = (\Omega_1, \Omega_2)$, where

$$\Omega_1 = p_1 + s_o p_2^2/2 \quad , \tag{39}$$

$$\Omega_2 = s_o p_1 p_2 \quad . \tag{40}$$

Because $s_o \ll 1$, the frequencies are generally well separated, $\Omega_1 \gg \Omega_2$, with Ω_2 vanishing at the rational surface, $p_2 = 0$. The resonance curves in action space are $\boldsymbol{\Omega}(\mathbf{p}) \cdot \mathbf{k} = \omega$, which are nearly parallel lines given by $p_1 = \omega/k_1$. Two modes whose wave vectors, $\mathbf{k}$, correspond to the same k_1, will have resonance curves which intersect in action space at the point $p_1 = \omega/k_1$ and $p_2 = 0$. When $s_o = 0$, Ω_2 vanishes everywhere and these resonances are degenerate, becoming a single straight line throughout action space. We will show below that the intersection of resonance curves in action space and their degeneracy when s_o vanishes, plays an important role in a particle's radial motion.

Since the motion is fast in the (p_1, z_1) plane compared to the (p_2, z_2) plane, it is convenient to define the "parallel Hamiltonian" as

$$H_{||} = \frac{p_1^2}{2} + \mathrm{Re}\{\sum_{k_1} A_{k_1} e^{i(k_1 z_1 - \omega t)}\} \quad , \tag{41}$$

$$A_{k_1} = \sum_{k_2} C_{\mathbf{k}}(\mathbf{p}) e^{ik_2 z_2} \quad , \tag{42}$$

where we consider z_2 and p_2 held fixed in the determination of the resonant amplitudes, A_{k_1}. (To obtain $H_{||}$ from H, one sets the slow frequency, Ω_2, identically to zero.) For given values of z_2 and p_2 one can obtain a two dimensional surface of section for the parallel dynamics. Since the motion is both periodic in z_1 and in time, t, one can either view the dynamics in the (p_1, z_1) phase plane at successive values in time spaced by $2\pi/\omega$, or in the $(H_{||}, t)$ plane at successive values of z_1 spaced by the periodicity length. One finds that the motion defined by $H_{||}$ becomes stochastic in the region of overlapping resonances given by the usual criterion

$$2(\sqrt{|A_\nu|} + \sqrt{|A_\mu|}) > \omega |\frac{1}{\nu} - \frac{1}{\mu}| \quad , \tag{43}$$

where the ν and μ are neighboring components of the k_1 spectrum and $4\sqrt{|A_{k_1}|}$ is the full trapping width of the resonance at $p_1 = \omega/k_1$.

We now consider the radial motion obtained from the Hamiltonian in (37) by differentiating with respect to the coordinate z_2:

$$\dot{p_2} = -\mathrm{Re}\{\sum_{k_1} B_{k_1} e^{i(k_1 z_1 - \omega t)}\} \quad , \tag{44}$$

where

$$B_{k_1} = \sum_{k_2} ik_2 C_{\mathbf{k}}(\mathbf{p}) e^{ik_2 z_2} \quad . \tag{45}$$

We may also consider the quasi-static limit where z_2 and p_2 are held fixed in B_{k_1}, so that the time rate of change of p_2, as given by (44), is completely determined by the orbit $z_1(t)$, which in turn is determined by the following:

$$\begin{aligned} \dot{z_1} &= p_1 \\ \dot{p_1} &= -\mathrm{Re}\{\sum_{k_1} ik_1 A_{k_1} e^{i(k_1 z_1 - \omega t)}\} \quad . \end{aligned} \tag{46}$$

Let us look at the radial motion of a particle trapped in the vicinity of a specific resonance. Ignoring all the non-resonant components of the spectrum, we consider only a single value

of k_1. We chose to write $B_{k_1} = ik_1 A_{k_1}(\beta e^{i\xi})$, where β and ξ are both real. Substituting this into (45) and using (42), one obtains

$$\beta e^{i\xi} = \frac{\sum_{k_2} k_2 C_{\mathbf{k}}(\mathbf{p}) e^{ik_2 z_2}}{k_1 \sum_{k_2} C_{\mathbf{k}}(\mathbf{p}) e^{ik_2 z_2}} \quad . \tag{47}$$

If there is only one finite term in each of the sums over k_2 in (47), then $\beta = k_2/k_1$ and $\xi = 0$. In the generic case, the spectrum will contain more than one Fourier component, $C_{\mathbf{k}}(\mathbf{p})$, at a given k_1, so that ξ will generally be non-zero; this corresponds to the intersection of two or more resonances in action space. Without loss of generality, we can chose $k_1 A_{k_1} = -\alpha$, where α is real and positive. Ignoring the sums over k_1 in equations (44) and (46), they can be written in the following form:

$$\dot{p}_2 = -\alpha\beta \sin(\varphi + \xi) \tag{48}$$

$$\ddot{\varphi} + \alpha \sin\varphi = 0 \quad , \tag{49}$$

where $\varphi = k_1 z_1 - \omega t$. The solution for $p_2(t)$ in terms of $\varphi(t)$ and $p_1(t)$ can be written as follows:

$$p_2(t) = p_2(0) + (\beta\cos\xi)\delta p_1(t) - (\alpha\beta\sin\xi)\int_0^t dt' \cos\varphi(t') \quad , \tag{50}$$

where $\delta p_1(t) = p_1(t) - p_1(0)$. Although $\delta p_1(t)$ is bounded by the trapping width of the resonance, the integral over $\cos\varphi(t)$ is clearly not bounded since for deeply trapped particles $|\varphi(t)| \leq \pi/2$. In this case the equations predict a secular drift in $p_2(t)$, i.e. $p_2(t) \sim -(\alpha\beta\sin\xi)t$ for times long compared to the bounce frequency of motion in the resonance. As particles approach the separatrix surrounding the resonance, $\cos\varphi(t)$ is negative for most of the time, so the drift changes direction. Generally, this secular drift cannot persist indefinitely, since after some time the quasi-static approximation is invalidated by the secularity, i.e. we no longer can consider z_2 and p_2 to be fixed in (47). In the specific case that $\sin\xi = 0$, the secular term in (50) vanishes and the excursion in $p_2(t)$ is proportional to $\delta p_1(t)$. Although the solution in (50) is not valid for long times when the secularity is present, it does show that the excursions in $p_2(t)$ are not generally restricted by the trapping width of the resonance. This effect gives rise to Arnold diffusion along an interconnected "web" of resonances when the amplitudes are too small to allow stochastic motion across the resonances [16].

V Quasilinear Diffusion During LHCD

When the spectral amplitudes of the wave field are large enough to satisfy the overlap criterion (43), yet small enough that their corresponding trapping widths are narrow compared to the width of the connected stochastic region, electrons in this region of phase space may be expected to diffuse quasilinearly. The quasilinear diffusion tensor in action space is [11]:

$$D_{i,j}(\mathbf{p}) = \sum_{\mathbf{k}} \frac{\pi}{2} |C_{\mathbf{k}}(\mathbf{p})|^2 \delta\left(\mathbf{\Omega}(\mathbf{p}) \cdot \mathbf{k} - \omega\right) k_i k_j \quad , \tag{51}$$

where the unperturbed frequencies, $\mathbf{\Omega}(\mathbf{p})$, are given in equations (39) and (40). (Note, that we have written the scalar potential as the real part of a complex Fourier series (38), so that its spectral energy is $|C_{\mathbf{k}}|^2/2$.) Although $D_{i,j}(\mathbf{p})$ is a singular tensor field it should be smoothed out by coarse-graining action space because the resonances are broadened by their trapping widths. Neglecting Ω_2 compared to Ω_1, we approximate the resonance condition as $p_1 \approx \omega/k_1$ and coarse grain in p_1 by averaging over an interval whose width is larger than the distance between resonances, but much smaller than the width of the stochastic region. The coarse-grained diffusion tensor is a function of $\mathbf{p}$; we will refer to this as the local diffusion tensor. The off diagonal elements of the local diffusion tensor are necessary in the Fokker-Planck operator to give the correct diffusion paths in $\mathbf{p}$ space. From (51) we can obtain a global estimate of the radial diffusion coefficient, $D_r = \langle D_{2,2}(\mathbf{p}) \rangle_{\mathbf{p}}$, where the averaging is over the entire stochastic region in $\mathbf{p}$ space. This global quantity is simply an indicator of the magnitude of the radial diffusion process which is described in detail by the local diffusion tensor. The quasilinear autocorrelation time, τ_{ql}, is

$$\tau_{ql} = \frac{\pi \langle k_1 \rangle}{\omega \Delta k_1} \quad , \tag{52}$$

where $\langle k_1 \rangle$ is the average value of k_1 over the spectrum whose width is Δk_1. Assuming that most of the spectral energy is located within the stochastic region, we may write D_r in the following way

$$D_r \approx \tau_{ql} \langle \sum_{\mathbf{k}} \frac{1}{2} k_2^2 |C_{\mathbf{k}}(\mathbf{p})|^2 \rangle_{p_2} \quad , \tag{53}$$

where $p_1 = \omega/k_1$ when it appears in $|C_{\mathbf{k}}(\mathbf{p})|^2$ and the final averaging is only over p_2. The global radial diffusion coefficient is converted into physical units by multiplying the expression in (53) by $(v_o/R_o)\rho_\theta^2$.

To evaluate the local diffusion tensor (51), or the global radial diffusion coefficient (53), we need to have an expression for the wave field inside the plasma. We consider that in the

core of the plasma, in the vicinity of r_o, there exists an ensemble of waves propagating in both the toroidal and poloidal directions and across flux surfaces. The potential is assumed to be of the following form:

$$\Phi = \mathrm{Re}\{\sum_{m,n} a_{m,n} e^{i(n\phi + m\theta + \kappa_{m,n} r - \omega t)}\} \quad , \tag{54}$$

where $\kappa_{m,n}$ is determined by assuming that ratio of parallel to perpendicular wave numbers is fixed by the local dispersion relation for high frequency (above the lower hybrid frequency) electrostatic waves. In particular, we take

$$\begin{aligned} k_{\|} &\approx (n + m/q_o) R_o^{-1} \\ k_{\perp} &\approx [\kappa_{m,n}^2 + (\frac{m}{r_o})^2]^{\frac{1}{2}} \quad , \end{aligned} \tag{55}$$

with $k_{\perp}/k_{\|}$ equal to the ratio of the local electron plasma frequency to the RF driving frequency [17]. Typically the spectrum launched into the plasma from the wave guide array is broad in n and vanishes outside the range $n_1 \leq n \leq n_2$; it is comparatively narrow in m and centered about $m = 0$. Although the results of toroidal ray tracing [18] and toroidal normal mode analysis [19, 20] show a significant upshift in the poloidal mode numbers of the spectrum inside the plasma, we will initially assume that the spectrum in the core is approximately the same as the spectrum launched into the plasma. In this case $k_{\|} \approx n/R_o$ and we can estimate n_2 from the condition that the lowest phase velocity in the spectrum, $\omega_{rf} R_o/n_2$, should intersect the tail of the central electron distribution function at about $4\sqrt{\mathrm{kT}/m_e}$, in order to drive sufficient current in the core of the plasma [21, 22]. For a frequency (f_{rf}) of about 2 GHz, in a 2.5 kev plasma with a major radius of 1 meter, this leads to $n_2 \approx 150$. In the following example we take $n_2 = 150$ and $n_1 = 100$, with $a_{m,n}$ identically vanishing outside of this range. Furthermore, we assume $a_{m,n}$ is finite only for $m = 0$. We now transform the potential (54) into action-angle coordinates using the transformation equations (27)-(29). We first note that $r = r_o + \rho_\theta \psi$ and rewrite (54) as

$$\Phi = \mathrm{Re}\{\sum_{n} a_n e^{i[n(\phi + \alpha\psi) - \omega t]}\} \quad , \tag{56}$$

where $\alpha = (k_{\perp}/k_{\|})(\rho_\theta/R_o)$. Since the RF frequency is on the order of the ion plasma frequency, we have $k_{\perp}/k_{\|} \sim \sqrt{m_i/m_e}$, so that $\alpha \sim \sqrt{m_i/m_e}\lambda\epsilon_o$. When using (28) and (29) to transform the combination $(\phi + \alpha\psi)$, there will be a term of order ϵ coming from the transfomation of ϕ and a term of order $\epsilon\alpha$ coming from the transformation of ψ. Since α is typically small we need only retain the order ϵ term which comes from transforming ϕ, so

we evaluate the potential at $\psi \approx -I_\theta/q_o$ (i.e. at an electron's average radial position). We find that

$$\phi + \alpha\psi \approx \zeta_\phi + \alpha p_2 - q_o\epsilon_o(1 - \frac{M}{p_1^2})\sin\zeta_\theta \quad , \tag{57}$$

where we have used the definitions of p_1 and p_2 given in (36). Substituting (57) into (56), one obtains the following relation for the Fourier components:

$$\begin{aligned} C_{n,l}(\mathbf{p}) &= a_n e^{in\alpha p_2}\left[\int \frac{d\zeta_\theta}{2\pi} e^{-il\zeta_\theta - inq_o\epsilon_o(1-M/p_1^2)\sin\zeta_\theta}\right] \\ &= a_n(-1)^l J_l\left(nq_o\epsilon_o(1-M/p_1^2)\right)e^{in\alpha p_2} \quad , \end{aligned} \tag{58}$$

where J_l is the ordinary Bessel function of order l. Using the definition of $\mathbf{k}$ following (38) we can change notation from $C_{n,l}(\mathbf{p})$ to $C_{\mathbf{k}}(\mathbf{p})$.

First consider $\epsilon_o = 0$, so that only the $l = 0$ coefficients in (58) are finite. Suppose we can write $|a_n|$ in terms of a smooth function for $n_1 \le n \le n_2$, i.e.

$$a_n = f(n)e^{i\xi_n} \quad , \tag{59}$$

where $f(n)$ is smooth and the phases, ξ_n, are randomly distributed. The coarse-grained diffusion coefficient, $D_{1,1}$, which follows from (51) can now be written as

$$D_{1,1}(p_1) = \frac{\pi\omega^2}{2p_1^3}[f(\frac{\omega}{p_1})]^2 \quad . \tag{60}$$

When $\epsilon_o = 0$ the other elements of the diffusion tensor vanish because p_2 is a conserved quantity. It is convenient to chose

$$f(n) = \Phi_o(\frac{n_1}{n})^{3/2} \quad , \tag{61}$$

so that $D_{1,1}$ in (60) is a constant. Chosing the velocity scale, $v_o = \omega_{rf}R_o/n_1$, so that $\omega = n_1$ (i.e. t is physical time normalized to $n_1\omega_{rf}^{-1}$) we find that $D_{1,1}(p_1) = (\pi/2)\Phi_o^2 n_1^2 \equiv D_o$. Note, that when $\Phi_o > (4n_1)^{-2}$, the overlap criterion is satisfied for $n_1/n_2 \le p_1 \le 1$, outside of which the diffusion coefficient drops from D_o to zero.

Assuming (61) and (59), and using (58), the quasilinear diffusion tensor for finite ϵ_o may be written as follows:

$$D_{i,j}(p_1) = D_o\sum_{l=l_1}^{l_2}\frac{k_1k_ik_j}{(k_1+k_2)^3}J_l^2(X) \tag{62}$$

where $k_1 = n_1/p_1$, $k_2 = -l/q_o$, $X = \epsilon_o q_o(k_1+k_2)(1-M/p_1^2)$, $l_2 = n_1q_o(1-p_1)/p_1$ and $l_1 = q_o(n_1 - n_2p_1)/p_1$. The limits on the l sum arise because $k_1 = n + l/q_o = n_1/p_1$ and a_n

vanishes for $n < n_1$ and $n > n_2$. Also the diffusion tensor is not a function of p_2, because we approximated the radial dependence of the RF field as $e^{ik_{m,n}r}$. The diffusion tensor (62) should be considered a local quantity defined in the vicinity of $p_2 = 0$, where $\epsilon = \epsilon_o$ and $q = q_o$. In Figure 1 we have plotted the elements of $D_{i,j}/D_o$ as functions of p_1 by numerically computing the sum in (62) for the case when $n_1 = 100$, $n_2 = 150$, $q_o = 2$, $\epsilon_o = .1$, and $M = 0$. It can be shown analytically that the central flat region of $D_{2,2}$ scales as $D_o\epsilon_o^2/2$. Figure 2 shows $D_{i,j}$ for the same parameters, except that $M = .2$. We see that although $D_{1,1}$ is nearly the same, $D_{1,2}$ and $D_{2,2}$ are significantly altered, since the factor $(1 - M/p_1^2)$ tends to reduce the argument of the Bessel functions in equation (58). Physically, the oscillation along a field line from the magnetic mirror tends to compensate for the shrinking of the parallel pathlength as particles rotate from the outside to the inside of the torus. For these examples, the basic scaling of the global radial diffusion coefficient, D_r, is obtained by substituting $k_2 \sim k_1\epsilon_o$ into (53). The resulting expression yields $D_r \sim D_o\epsilon_o^2$. Clearly, if the poloidal mode numbers, m, are large enough (as when they upshift due to toroidal effects on wave propagation) there will be an enhancement in the radial diffusion coefficient over the above example with m identically zero. One finds that for $|m| \gg q_o\epsilon_o n$ the dominant terms in the radial diffusion are obtained by ignoring the order ϵ effects altogether; in this case D_r becomes the usual expression for $E \times B$ diffusion induced by a poloidal electric wave field. We note that the $E_\phi \times B_\theta$ drift is one order of ϵ smaller than the drift induced via the parallel electric field by coupling to the equilibrium ∇B and curvature drifts. Consequently, the $E_\phi \times B_\theta$ drift is ignored because we have truncated the action-angle transformation to first order in ϵ.

The quasilinear diffusion can be compared to that observed by numerically following the exact orbits of an ensemble of particles whose initial conditions are at the same point in action space and uniformly distributed throughout the range of both angles. We introduce the following diagnostic quantity:

$$d_{i,j}(t; \mathbf{p}_o) = \frac{\langle p_i(t)p_j(t)\rangle - \langle p_i(t)\rangle\langle p_j(t)\rangle}{2tD_o} \tag{63}$$

where $\mathbf{p}(0) = \mathbf{p}_o$ and the angular brakets indicate an ensemble average. In Figures 3 and 4 we show $d_{i,j}(t; \mathbf{p_o})$ for $\Phi_o = 10^{-5}$ and two different values of $p_1(0)$. The other parameters are the same as given above for Figure 1. We can identify two time scales on which $d_{i,j}(t)$ varies: the fastest is τ_{ac}, the time required for the autocorrelation function of $p_1(t)$ to decay, the slow time scale is τ_d, which is the time required for the ensemble to spread across the stochastic region, or the diffusion time. The time τ_{ac} can be distinguished in Figures 3 and 4 as the time it takes for the initial transient in $d_{i,j}(t)$ to decay, i.e. $\tau_{ac} \lesssim 1$. The quasilinear

estimate of τ_{ac} is given by τ_{ql} in (52) (for this example, $\omega \sim \langle k_1 \rangle$ and $\Delta k_1 \sim 50$, giving $\tau_{ql} \sim .1$). For times long compared to τ_{ac}, but short compared to τ_d, Figures 3 and 4 show that $d_{i,j}(t; \mathbf{p_o}) \approx D_{i,j}(p_1(0))/D_o$, where the quasilinear diffusion tensor is given by equation (62) and is shown in Figure 1. The diffusion time for these parameters is quite long, on the order of 10^4, because D_o is so small (approximately 10^{-6}). In Figure 3, one sees that the transient portion of $d_{1,2}(t)$ persists much longer than those of the diagonal components of $d_{i,j}(t)$. We note that in the case of Figure 3, we chose $p_1(0) = .8$, which corresponds to the central flat region of $D_{i,j}(p_1)$ where $D_{1,2}$ nearly vanishes. When $p_1(0)$ is chosen towards the outer portion of the stochastic region, where $D_{1,2}(p_1)$ is large, the transient portion of $d_{1,2}(t)$ decays faster, as shown in Figure 4. From the Figures one can also identify smaller transients in $d_{i,j}(t)$ which take place on a longer time scale than τ_{ac}, but are still fast compared to τ_d. This intermediate time scale, which we define as τ_r, can be identified as the time required for the ensemble to spread in p_1 across the width between two neighboring resonances. The time scale, τ_r, arises generically when analyzing diffusion in two-dimensional stochastic maps with periodicity in only one direction, such as the Fermi map [23].

Having established the connection between the diffusion predicted by the local quasilinear tensor and that observed numerically, it is interesting to go back and look at the scaling for radial diffusion given by D_r in (53). In terms of the average parallel electric wave field

$$E_{||}^2 = (\frac{mv_o^2}{eR_o})^2 \langle \sum \frac{1}{2} k_1^2 |C_{\mathbf{k}}(\mathbf{p})|^2 \rangle_{p_2} \quad , \tag{64}$$

we can write the radial diffusion coefficient in physical units as

$$D_{rad} \sim \frac{\langle k_1 \rangle E_{||}^2}{2 f_{rf} \Delta k_1 B_o^2} \langle\langle (\frac{k_2 B_o}{k_1 B_\theta})^2 \rangle\rangle \quad , \tag{65}$$

where $D_{rad} \equiv D_r (v_o/R_o)\rho_\theta^2$ and the double brackets indicate an averaging over both the spectrum (weighted by the spectral energy) and the radial coordinate. For $\langle k_1 \rangle \approx \Delta k_1$, $f_{rf} \approx 2$ GHz and $B_o \approx 5$ Tesla, one finds that $D_{rad} \sim (.1\mathrm{m}^2/\mathrm{sec}) E_{||}^2 \langle\langle (k_2 B_o/k_1 B_\theta)^2 \rangle\rangle$, where $E_{||}$ is expressed in kV/cm. In the example problem, where we assumed that the poloidal mode numbers were identically zero, the term enclosed by double brackets is of order unity. For upshifted poloidal mode numbers, this term could be as large as $(B_o/B_\theta)^2$. Thus with large wave fields, $E_{||} \gtrsim .1$kV/cm, quasilinear scaling can yield an appreciable RF induced radial diffusion. However at such large amplitudes, the typical trapping widths of individual resonances are on the order of the width of the stochastic region and the quasilinear approximation is invalid. For example, in Figure 3, $\Phi_o = 10^{-5}$ corresponding to

an $E_{||}$ of about 10^{-3}kV/cm and a trapping width ($4\sqrt{\Phi_o}$) of about 1.3×10^{-2}. Increasing Φ_o by two orders of magnitude results in a trapping width that is about one fourth of the width of the stochastic interval in p_1.

VI Stochasticity And Diffusion From A Few Large Amplitude Waves

In this section we assume that the potential is given by (54), where m and n are the same order of magnitude. Ignoring the order ϵ piece of the action-angle transformation we write the potential as

$$\Phi = \sum \Phi_{\mathbf{k}} \cos(\mathbf{k} \cdot \mathbf{z} + \alpha_{\mathbf{k}} p_2 - t) \quad , \tag{66}$$

where $k_1 = (n + m/q_o)/n_o$, $k_2 = -m/(n_o q_o)$, $\alpha_{\mathbf{k}} = \rho_\theta \kappa_{m,n}$, and n_o is some typical toroidal mode number of the wave spectrum. The Hamiltonian has the same form as in equation (37), where we have rescaled the coordinates z_1 and z_2 by the factor n_o; t is physical time normalized to ω_{rf}^{-1} and the velocity scale is $v_o = \omega_{rf} R_o/n_o$. Noting that $\rho_\theta = v_o B_\phi/\omega_{ce} B_\theta$ and $q_o R_o/r_o = B_\phi/B_\theta$, and using (55), one obtains

$$\alpha_{\mathbf{k}} = \frac{k_\perp \omega_{rf} B_\phi}{k_{||} \omega_{ce} B_\theta} [k_1^2 - (\frac{B_\phi k_{||}}{B_\theta k_\perp})^2 k_2^2]^{\frac{1}{2}} \quad , \tag{67}$$

Typical parameter values are: $(k_\perp/k_{||})^2 \sim 10^3$, $B_\phi/B_\theta \sim 10$, and $\omega_{ce}/\omega_{rf} \sim 10^2$. Using these one finds that $\alpha_{\mathbf{k}} \sim \sqrt{10k_1^2 - k_2^2}$. In the following we consider the stochasticity and radial transport induced by just a few such modes, where the spacing between the k_1 mode numbers is on the same order as k_1. In this situation the amplitude of the waves must be large to satisfy the overlap criterion and the width of the stochastic interval in p_1 is on the order of a few resonant trapping widths.

We first consider the case of just three modes, since for fewer modes than this there will always exist at least one constant of the motion. In particular we take: $\Phi_k = \Phi_o$ for $\mathbf{k} = (1.5, -.5)$, $(2, -1)$, and $(3, -1)$, where Φ_o is real and positive. Recall that the resonance condition is $\mathbf{\Omega}(\mathbf{p}) \cdot \mathbf{k} = 1$, where the unperturbed frequencies are given in equations (39) and (40). Since $\Omega_2 \ll \Omega_1$, the resonance condition is $p_1 \approx 1/k_1$, so that the resonances for these modes occur at $p_1 = 1/3$, $1/2$, and $2/3$, respectively. Each point in the (p_2, z_2) plane can be associated with a two-dimensional parallel Hamiltonian as defined in (41). We see that $|A_{k_1}| = \Phi_o$, where A_{k_1} is defined in (42), so that the overlap criterion in (43) is satisfied

when $\Phi_o > 1.7 \times 10^{-3}$. The (p_1, z_1) surface of section for the parallel Hamiltonian is shown in Figure 5 for the case when $\Phi_o = 2 \times 10^{-3}$. Since $|A_{k_1}|$ is independent of p_2 and z_2, the parallel surface of section is similar at all points in the (p_2, z_2). We now let the coordinates p_2 and z_2 evolve according to the complete Hamiltonian dynamics, as opposed to being held constant in the above two-dimensional surface of section. For example, Figure 6 shows the time series, $p_1(t)$ and $p_2(t)$, of a typical stochastic orbit when $\Phi_o = 10^{-2}$. In this case $p_2(t)$ shows a fast stochastic variation superimposed upon a slow meandering. Focusing in on the fast stochastic motion, one can see that it is directly correlated to the p_1 time series. We showed in Section IV, following equation (50), that for motion in the vicinity of any non-degenerate resonance the excursions in p_1 and p_2 are proportional by the ratio of k_1/k_2. Since this ratio varies as the orbit jumps stochastically from one resonance to another, the overall time series for the two actions will not be proportional. Averaging over the fast stochastic variations one sees that the mean of p_2 tends to wander, whereas p_1 is confined to the region of overlapping resonances. Varying the shear parameter, s_o, does not have a significant effect on either the p_1 or p_2 time series in this example.

We now add a fourth mode to the spectrum in the above example. The additional mode is chosen in such a way as to create a degenerate resonance. In particular we take: $\Phi_k = \Phi_o$ for $\mathbf{k} = (1.5, -.5)$, $(2, -1)$, $(2, 0)$ and $(3, -1)$, where Φ_o is real and positive. For the set of modes in the first example, the resonance curves were non-degenerate, in the sense that each A_{k_1} was composed of only a single mode in the sum over k_2. On the other hand, in the present example, the resonance curves for the two modes with equal k_1 components, (2,0) and (2,-1), intersect at the point $p_1 = 1/2$ and $p_2 = 0$. In the limit of vanishing Ω_2, the resonances for these two modes coalesce throughout action space creating a degenerate resonance at $p_1 = 1/2$. We define Φ_d as the potential obtained by explicitly adding the two degenerate modes. Using the notation $\mathbf{k} = (k_1, k_2)$ and $\mathbf{k}' = (k_1, k_2')$ for the two degenerate modes, one can write Φ_d as follows:

$$\Phi_d = 2\Phi_o \cos\vartheta \cos\left(k_1 z_1 + \bar{\alpha} p_2 + \bar{k}_2 z_2 - t\right) \quad , \tag{68}$$

where

$$\vartheta = \frac{(k_2' - k_2)}{2} z_2 + \frac{(\alpha_{\mathbf{k}'} - \alpha_{\mathbf{k}})}{2} p_2 \quad , \tag{69}$$

$\bar{k}_2 = (k_2 + k_2')/2$, and $\bar{\alpha} = (\alpha_{\mathbf{k}} + \alpha_{\mathbf{k}'})/2$. The amplitude of the degenerate resonance is $2\Phi_o|\cos\vartheta|$, which depends on a particles position coordinates in the (p_2, z_2) plane as given by ϑ in (69). For the four mode example, the (p_1, z_1) surface of section of the parallel

Hamiltonian is shown in Figure 7 for two different positions in z_2 at $p_2 = 0$ and with $\Phi_o = 2 \times 10^{-3}$. In Figure 7a, the amplitude of the degenerate resonance vanishes because $\vartheta = \pi/2$ and the phase space is dominated by the remaining two resonances at $p_1 = 1/3$ and $2/3$. At this value of Φ_o the trapping widths of these resonances do not overlap and we see that they are seperated by phase spanning KAM curves in the surface of section. In Figure 7b, the degenerate resonance has nearly the same amplitude as the other two and the overlap criterion is satisfied forming a thick layer of stochasticity. At larger values of Φ_o, greater than about 7×10^{-3}, the trapping widths of the $p_1 = 1/3$ and $2/3$ resonances overlap. In this case a stochastic layer in parallel phase space is seen at all values of p_2 and z_2.

We continue our analysis of the four wave example by looking at the time series determined from the four-dimensional Hamiltonian. Figure 8 shows a typical stochastic orbit for $\Phi_o = 10^{-2}$ and $s_o = 0$; we see that $p_2(t)$ and $z_2(t)$ exhibit fluctuations about a uniform average drift. The origin of this streaming motion is related to the degenerate resonance as explained in Section IV following equation (50). The direction of the stream depends on the initial conditions in the (p_2,z_2) plane. It is possible to show that the streaming motion progresses along a line in the (p_2, z_2) plane, because ϑ in (69) is approximately conserved by the Hamiltonian dynamics with zero shear. This can be determined from the equations of motion by using the potential Φ_d given in (68) and ignoring the additional contributions of the two non-degenerate waves to the total potential; one finds that ϑ is proportional to $p_1(t)$, so that with $p_1(t)$ bounded to the region of overlapping resonances the streaming must approximately conserve ϑ. In addition the streaming can move in either direction along a line of constant ϑ depending on the the initial value of ϑ in Φ_d. When shear is included, the streaming motion cannot persist since ϑ is no longer approximately conserved. Figure 9 shows the time series for the same initial condition as in Figure 8, but with $s_o = 10^{-2}$. We see that $p_2(t)$ moves stochastically in a random walk fashion. As soon as p_2 becomes appreciable, the time dependence of z_2 is dominated by the linear frequency (i.e. $\dot{z}_2 \approx \Omega_2$, where $\Omega_2 = s_o p_1 p_2$). We note that the excursions in p_2 are no longer approximately proportional to the excursions in p_1, as was the case in the example with three non-degenerate resonances (see Figure 6). In fact we can see directly by comparing the $p_2(t)$ time series in Figures 6 and 9, that the radial excursions are significantly enhanced by the presence of intersecting resonances.

For stochastic orbits, the power spectra of the p_1 time series obtained from the four-

dimensional Hamiltonian are the same as those obtained from the two-dimensional parallel Hamiltonian. The parallel Hamiltonian provides a useful way of visualizing the actual parallel dynamics which is really a projection onto the (p_1, z_1) plane of motion in a four-dimensional phase space. Regular orbits, or "sticky" orbits initially near invariant surfaces of the parallel Hamiltonian are significantly altered by the four-dimensional dynamics. In the four-dimensional case the invariant surfaces seen in the Figure 7 no longer isolate portions of the (p_1, z_1) plane. For example, chosing an initial condition in the small primary island of the degenerate resonance at $p_1 = 1/2$ (see Figure 7b), we know that in the two-dimensional case the orbit remains regular and is confined within this structure. Figure 10 shows the time series obtained from the four dimansional Hamiltonian for the same initial condition. We see that after many oscillations the orbit becomes stochastic. Although the orbit appears quasi-periodic while it is trapped in the island structure, only a small amount of Arnold diffusion is required for the orbit to escape into the stochastic region of the (p_1, z_1) plane. Consider the same initial condition, but now with $s_o = 0$, as in Figure 11. In this case, although we see aperiodic behavior in $p_1(t)$, the orbit never escapes the island, during which time it streams uniformly in the (p_2, z_2) plane. It is also interesting to compare the time series in $p_2(t)$ for two stochastic orbits, one at higher amplitude, as previously shown in Figure 9, and one at lower amplitude, as in Figure 12 (both with finite shear). In the lower amplitude case the motion is characterized by sharp jumps in p_2 intermingled with smaller scale fluctuations; basically the orbit spends long periods of time in the vicinity of each of the resonances as it stochastically moves from one to the other; when stuck in the vicinity of the intersecting resonances (i.e. the degenerate resonance when s_o vanishes), the orbit makes a large excursion in p_2. At larger amplitude the relative sharpness of these excursions fades, since the overall stickyness to any particular resonance is reduced.

To assess the radial transport induced by the waves, we consider the evolution of an ensemble of initial conditions. The ensemble is initially located at a specific p_2, z_2, and p_1, but uniformly spread in z_1 across a region of stochastic phase space. In particular we have chosen 1280 initial conditions at $p_2 = 0$, $z_2 = \pi/2$, $p_1 = .43$, and $0 < z_1 \leq 4\pi$ corresponding to a stochastic strip in the (p_1, z_1) surface of section. The ensemble is allowed to evolve in time according to the equations of motion. The mean of the distribution, $\bar{p}_2(t)$, and the variance, $\sigma(t)$, are defined in the usual way: $\bar{p}_2(t) = \langle p_2(t) \rangle$ and $\sigma(t) = \langle p_2(t)^2 \rangle - \langle p_2(t) \rangle^2$, where the angular brackets denote ensemble averages. We will first discuss the results with finite shear ($s_o = 10^{-2}$). For long times, the mean is stationary and the variance grows

SPECTRUM $\mathbf{k} = (k_1, k_2)$	Φ_o	γ	σ_o
Three Waves			
$\mathbf{k} = (1.5, -.5), (2, -1), (3, -1)$	10^{-2}	1.0	5×10^{-6}
Four Waves			
$\mathbf{k} = (1.5, -.5), (2, -1), (2, 0), (3, -1)$	10^{-2}	1.0	1×10^{-4}
	2×10^{-3}	0.9	5×10^{-5}

Table 1: Results for three wave and four wave examples; $\sigma(t) \approx \sigma_o t^\gamma$, where $\sigma(t) = \langle p_2(t)^2 \rangle - \langle p_2(t) \rangle^2$. When $\gamma = 1$ the radial motion is a random walk and the diffusion coefficient in physical units is $\sigma_o \pi f_{rf} \rho_\theta^2$. Additional parameters are $s_o = 10^{-2}$ and $\alpha_\mathbf{k} = (10k_1^2 - k_2^2)^{1/2}$ following equation (67).

proportional to a power of time, i.e. $\sigma(t) \approx \sigma_o t^\gamma$. By "long times" we mean long compared to the time required for the ensemble to spread over the stochastic interval in p_1 and long compared to the time required for the ensemble to mix throughout the range of z_2. On the other hand, the time cannot be so long that the ensemble has spread beyond the range of the local shear, i.e. $s_o \langle |p_2| \rangle \ll 1$. In this sense, the observed power law behavior for $\sigma(t)$ is not truely asymptotic, but rather it is applicative only over a range of times. Note, that $\alpha_\mathbf{k} \gg s_o$ so that for "long times" the ensemble has typically spread over a region large enough to sample the fast variation of the wave field with respect to p_2. For "long times" the results are independent of the ensemble's initial conditions, as long as they are located in the stochastic region of the (p_1, z_1) plane. For the four wave spectrum at large amplitude ($\Phi_o = 10^{-2}$), we find that $\gamma = 1.0$ and $\sigma_o = 1 \times 10^{-4}$; $\sigma(t)$ is shown in Figure 13, where the linear regime (i.e. $\sigma = \sigma_o t^\gamma$) is for $t/2\pi \gtrsim 10^3$. When γ is unity, the motion in p_2 is a classical random walk with a diffusion coefficient of $\sigma_o/2$. At smaller amplitude ($\Phi_o = 2 \times 10^{-3}$), the exponent in the power law for $\sigma(t)$ decreases; $\gamma = 0.9$ and $\sigma_o = 5 \times 10^{-5}$. Comparing this to the initial three wave spectrum, where there was no degenerate resonance, one finds a sharp decrease in the radial transport: for example at $\Phi_o = 10^{-2}$, $\gamma = 1.0$ and $\sigma_o = 5 \times 10^{-6}$. The results are summarized in Table 1. For the four wave example with $\Phi_o = 10^{-2}$, if we take $\rho_\theta \sim 10^{-3}$m for energetic electrons and $f_{rf} \sim 2GHz$, the radial diffusion in physical units ($\sigma_o \pi f_{rf} \rho_\theta^2$) is about 1 m^2/sec.

In the four wave example, the results with s_o zero are dramatically different because of the streaming orbits. In general, we observe either the entire ensemble, or part of it, streaming along a line of constant ϑ in the (p_2, z_2) plane. For example, at $\Phi_o = 10^{-2}$, in the case with zero shear we see $\bar{p}_2(t) \approx \mu t$, where the magnitude and sign of μ depend on the ensemble's initial value of ϑ. For an ensemble initially at $\vartheta = \pi/4$, we find that

$\mu \approx -3 \times 10^{-4}$. Compare this to the case with finite shear shown in Figure 14; for a short time $\bar{p}_2(t)$ streams negatively at a relatively uniform rate, at $t/2\pi \approx 250$ the slope of $\bar{p}_2(t)$ abruptly changes sign and it streams positively until $t/2\pi \approx 500$, after which it breaks into a fluctuating state with no average time rate of change. The effect of shear is to make $\Omega_2(\mathbf{p})$ finite for orbits which move away from the rational surface at $p_2 = 0$. In Figure 15, we show the ensemble averaged variance in z_2 as a function of time for the case with $s_o = 10^{-2}$. (The variance in z_2 is defined as $\langle z_2(t)^2 \rangle - \langle z_2(t) \rangle^2$). The long time dependence of the z_2 variance is a power law with an exponent of 3. This power law is predicted by integrating $\dot{z}_2 \approx s_o p_1 p_2$ with $p_1 \approx$ constant and with $p_2 \approx \pm\sqrt{\sigma_o t}$, as given by the effective random walk in p_2, and then squaring to form $\langle z_2(t)^2 \rangle$. When the shear is zero, the variance in z_2 ceases to spread after an initial transient which corresponds to the spreading of the ensemble throughout the stochastic region in p_1. In the lower amplitude case, $\Phi_o = 2 \times 10^{-3}$, Figure 16 shows two distributions in p_2 of ensembles initially started at $p_2 = 0$ and allowed to evolve until $t/2\pi = 10^4$: one is for $s_o = 10^{-2}$ and the other for $s_o = 0$. While the case with shear shows an evenly spread distribution function (whose variance is growing as $t^{0.9}$), the case with zero shear shows a long negative tail. This tail forms because of the fast streaming motion of particles which get stuck in the primary island of the degenerate resonance in the (p_1, z_1) plane, since at this amplitude the primary resonance still retains a stable fixed point as shown in Figure 7b. In the four-dimensional dynamics, a particle's motion in the (p_2, z_2) plane, allows it to pass in and out of such islands. Thus, even though all initial conditions are chosen in the stochastic region, the island gradually acquires a small population of steaming particles.

VII Conclusions

The Lagrangian formulation of guiding center motion provides an elegant and powerful method for deriving canonical coordinates in toroidal geometry. Although an explicit transformation between toroidal coordinates and action-angle coordinates cannot generally be obtained, it is possible to obtain an approximate transformation by exploiting the fact that the deviation of an electron's orbit from its average flux surface is small compared to the scale length of the equilibrium magnetic inhomogeneity. The straight forward expansions used in the text provide an explicit representation for the Hamiltonian in action-angle coordinates that is valid for circulating particles in the vicinity of a given flux surface. This

is given by the unperturbed Hamiltonian in (24) and the transformation equations, (27) through (29), which are needed to obtain the wave field in action-angle coordinates. In the action-angle representation both the wave induced $E \times B$ drift and the radial motion that arises from the coupling of the wave induced parallel acceleration to the equilibrium toroidal drift, occur at the same level of description, i.e. they simply result in different components of the wave field's action-angle spectrum. Once the poloidal electric field of the wave is large enough (approximately $|m| > \epsilon qn$), the dominant mechanism for radial transport is the wave induced $E \times B$ drift.

The unperturbed frequencies, $\Omega_\phi(\mathbf{I})$, and $\Omega_\theta(\mathbf{I})$ of the action-angle coordinates are nearly proportional except for a small term which arises due to the shear of the magnetic field lines. A simple linear transformation defined by (36) yields a new canonical coordinate system, $(\mathbf{p}, \mathbf{z})$, whose unperturbed frequencies satisfy the ordering $\Omega_1(\mathbf{p}) \gg \Omega_2(\mathbf{p})$. The frequency $\Omega_2(\mathbf{p})$ vanishes at $p_2 = 0$, which corresponds to some rational q surface in the plasma. The Hamiltonian expressed in $(\mathbf{p}, \mathbf{z})$ coordinates, as given in (37), describes the dynamics in the vicinity of this rational surface. Because of the seperation between Ω_1 and Ω_2, the four-dimensional phase space naturally divides into two coupled two dimensional phase planes: (p_1, z_1) and (p_2, z_2), where the motion in the first plane is fast compared to the second. Holding the coordinates p_2 and z_2 fixed, we define an effective two dimensional Hamiltonian, $H_{||}$, as in (41). The stochastic threshold determined by $H_{||}$ occurs when the wave spectrum satisfies the usual overlap criterion, as given by (43).

For a broad spectrum of randomly phased waves, with closely spaced resonances whose trapping widths overlap, we have measured the stochastic diffusion in $\mathbf{p}$ space and compared it with the local quasilinear diffusion tensor evaluated for the same spectrum. For wave fields large enough that the quasilinear radial diffusion becomes appreciable, the trapping widths of individual resonances extend over a large portion of the stochastic region. Our initial investigations of this large amplitude regime indicate a dramatic reduction of the radial diffusion in comparison to the quasilinear value; more numerical work is needed to determine the scaling of the radial diffusion with respect to the wave amplitude. We are currently considering the case when the wave modes are not randomly phased and the field is represented by a spatially localized wave packet.

For the case when stochasticity is induced by a few large amplitude waves, we find that the radial transport is greatly enhanced when the wave-particle resonance curves intersect

in action space. When resonances do not intersect, the excursions in p_2 are always nearly proportional to the excursions in p_1, where the latter are bounded by the trapping widths of the resonances. When resonances intersect, excursions in p_2 are greatly enhanced, even though the stochastic motion in p_1 looks very similar. Without shear, the intersecting resonances become degenerate and we find that stochastic trajectories stream in the (p_2, z_2) plane. At large amplitudes, an ensemble of trajectories, initially at the same point in the (p_2, z_2) plane and spread throughout the stochastic region in the (p_1, z_1) plane, will stream at a uniform rate, i.e. $\langle p_2(t) \rangle \approx \mu t$, where μ depends on the initial condition in the (p_2, z_2) plane. At lower amplitudes, where the primary resonances of the parallel Hamiltonian still retain stable fixed points, some trajectories in the ensemble get trapped by the degenerate resonance; their corresponding streaming motion creates a long tail to the ensemble's radial distribution, as shown in Figure 16. With small but finite shear, the streaming motion does not persist and the resulting transport in p_2 is diffusive; in the large amplitude case we find a diffusion coefficient of about 1 m^2/sec (see Table 1). At lower amplitudes the transport is slower than would be given by a classical random walk. In general we find that after an initial transient, the growth in the mean square of p_2 is proportional to a power of time; at lower amplitudes the exponent is below unity. We are currently in the process of obtaining the scaling of this relation with respect to wave amplitude.

VIII Acknowledgements

We wish to acknowledge fruitful discussions with Dr. Dieter J. Sigmar. This work was supported in part by National Science Foundation Grant No. ECS-88-2475 and in part by U.S. Department of Energy Contract No. DE-AC02-78ET-51013.

References

[1] R.K. Kirkwoood, PhD Thesis Department of Nuclear Engineering, Massachusetts Institute of Technology, Cambridge, MA (September 1989); Phys. Fluids B (to appear in June, 1990).

[2] V. Fuchs, V. Krapchev, A.K. Ram, and A. Bers, Physica **14D** 141 (1985).

[3] G.M. Zaslavskii, Sov. Phys. JETP 61 (1985) 1176.

[4] A.K. Ram, A. Bers, K. Kupfer, Phys. Lett. A **138**, 288 (1989).

[5] R.G. Kleva, J.F. Drake, Phys. Fluids **27**, 1686 (1984).

[6] W. Horton, D.I. Choi, Plasma Phys. and Contr. Fusion **29**, 901 (1987).

[7] K. Kupfer, A. Bers, A.K. Ram, *Proceedings of the Eighth Topical Conference on RF Plasma Heating*, May 1-3, 1989, Irvine, CA, A.I.P. Conf. Proc. 190 (R. McWilliams, ed.) New York, pp. 434-437.

[8] R.G. Littlejohn, J. Plasma Phys. **29** 111 (1983).

[9] T.M. Antonsen, Jr., K. Yoshioka, Phys. Fluids **29**, 2235 (1986).

[10] K.C. Shaing, Phys. Fluids **31**, 2249 (1988).

[11] A.N. Kaufman, Phys. Fluids **15**, 1063 (1972).

[12] A.H. Boozer, Phys. Fluids **27**, 2441 (1984).

[13] J.P. Freidberg, *Ideal Magnetohydrodynamics*, Plenum Press (New York, 1987).

[14] R.B. White, M.S. Chance, Phys. Fluids **27**, 2455 (1984).

[15] L.D. Landau, E.M. Lifshitz, *Mechanics*, Pergamon Press (New York, 1976).

[16] A.J. Lichtenberg, M.A. Lieberman, *Regular and Stochastic Motion*, Springer-Verlag (New York, 1983).

[17] A. Bers, *Proceedings of the Third Topical Conference on RF Plasma Heating*, Jan. 11-13, 1978, California Institute of Technology, Pasadena, CA, pp. A1:1-10.

[18] P.T. Bonoli, R.C. Englade, Phys. Fluids **29**, 2937 (1986).

[19] D. Moreau, Y. Peysson, J.M. Rax, A. Samain, J.C. Dumas, Nucl. Fusion **30**, 97 (1990).

[20] D. Moreau, J.M. Rax, A. Samain, Plasma Phys. and Contr. Fusion **31**, 1895 (1989).

[21] N.J. Fisch, Phys. Rev. Lett. **41**, 873 (1978)

[22] V. Fuchs, R.A. Cairns, M.M. Shoucri, K. Hizanidis, A. Bers, Phys. Fluids **28**, 3619 (1985).

[23] A.J. Lichtenberg, M.A. Lieberman, *Diffusion In Two Dimensional Mappings*, Electronics Research Laboratory Memorandum No. UCB/ERL M88/5, University of California, Berkeley (1988).

Appendices

A The Sheared Slab

Here we derive canonical coordinates for a magnetized slab with shear. The vector potential is chosen to be

$$\mathbf{A} = B_o(x\hat{y} - \frac{x^2}{2L_s}\hat{z}) \quad , \tag{70}$$

so that the magnetic field is

$$\mathbf{B} = B_o(\hat{z} + \frac{x}{L_s}\hat{y}) \quad , \tag{71}$$

where L_s is the length scale of the shear. Substituting these into the Lagrangian in equation (1) one obtains the canonical momenta:

$$p_z = u\frac{B_o}{B(x)} - s\frac{x^2}{2} \quad , \tag{72}$$

$$p_y = x(1 + su\frac{B_o}{B(x)}) \quad , \tag{73}$$

where the Hamiltonian is

$$H = \frac{u^2}{2} + MB(x) + \Phi(x, y, z, t) \quad . \tag{74}$$

The units of velocity are v_o and the units of time are ω_c^{-1}, where $\omega_{ce} = eB_o/m$. The units of distance are ρ_o, defined as v_o/ω_{ce}, and $s \equiv \rho_o/L_s \ll 1$. Noting that $u = p_z + sp_y^2/2 + \mathcal{O}s^2$, and $B(x) = 1 + \mathcal{O}s^2$, by ignoring terms of order s^2 one obtains

$$H_o = \frac{p_z^2}{2} + sp_z\frac{p_y^2}{2} \quad , \tag{75}$$

which is the unperturbed Hamiltonian in equation (37). The potential $\Phi(x, y, z, t)$ can be written in the canonical coordinates most simply by exchanging x for p_y and ignoring terms of order $s\partial\Phi/\partial x$, which arise through equation (73).

Note, the unperturbed Hamiltonian system is invariant under the following scale transformation: $z = aZ$, $y = bY$, $t = aT$, $p_y = (a/b)P_y$, and $p_z = P_z$. The equations of motion in the lower case and upper case variables are identical if one rescales the shear parameter as $S = (a/b)^2 s$. The scale used in the text is obtained by making the assignment $b = q_o r_o/\rho_o$ and $a = R_o/\rho_o$, where upon we may interpret Z as z_1, Y as z_2, and the parameter S as s_o.

B Guiding Center Equations in Toroidal Coordinates

Here we obtain the equations of motion in the coordinates $(\rho_{\|}, \psi, \theta, \phi)$, where $\rho_{\|} \equiv u/B$. By directly applying the Euler-Lagrange equations to the Lagrangian in (8), where p_θ and p_ϕ are functions of ψ, θ, and $\rho_{\|}$, one obtains the four equations of motion:

$$\dot{\phi} = \mathcal{J}^{-1}[(G' - \rho_{\|}F')\frac{\partial H}{\partial \rho_{\|}} + F\frac{\partial H}{\partial \psi}] \tag{76}$$

$$\dot{\theta} = \mathcal{J}^{-1}[(1 + \rho_{\|}g')\frac{\partial H}{\partial \rho_{\|}} - g\frac{\partial H}{\partial \psi}] \tag{77}$$

$$\dot{\rho_{\|}} = -\mathcal{J}^{-1}[(1 + \rho_{\|}g')\frac{\partial H}{\partial \theta} + (G' - \rho_{\|}F')\frac{\partial H}{\partial \phi}] \tag{78}$$

$$\dot{\psi} = \mathcal{J}^{-1}[g\frac{\partial H}{\partial \theta} - F\frac{\partial H}{\partial \phi}] \quad , \tag{79}$$

where

$$\mathcal{J} = F(1 + \rho_{\|}g') + g(G' - \rho_{\|}F') \quad . \tag{80}$$

The prime superscript indicates differentiation with respect to ψ and the Hamiltonian, H, is considered a function of $\rho_{\|}$, ψ, θ, and ϕ, as given by

$$H = \frac{1}{2}{\rho_{\|}}^2 B^2(\psi, \theta) + MB(\psi, \theta) + \Phi(\psi, \theta, \phi, t) \quad . \tag{81}$$

$\mathcal{J}$ is the Jacobian of the coordinate transformation from the canonical momenta p_θ and p_ϕ to the non-canonical coordinates ψ and $\rho_{\|}$.

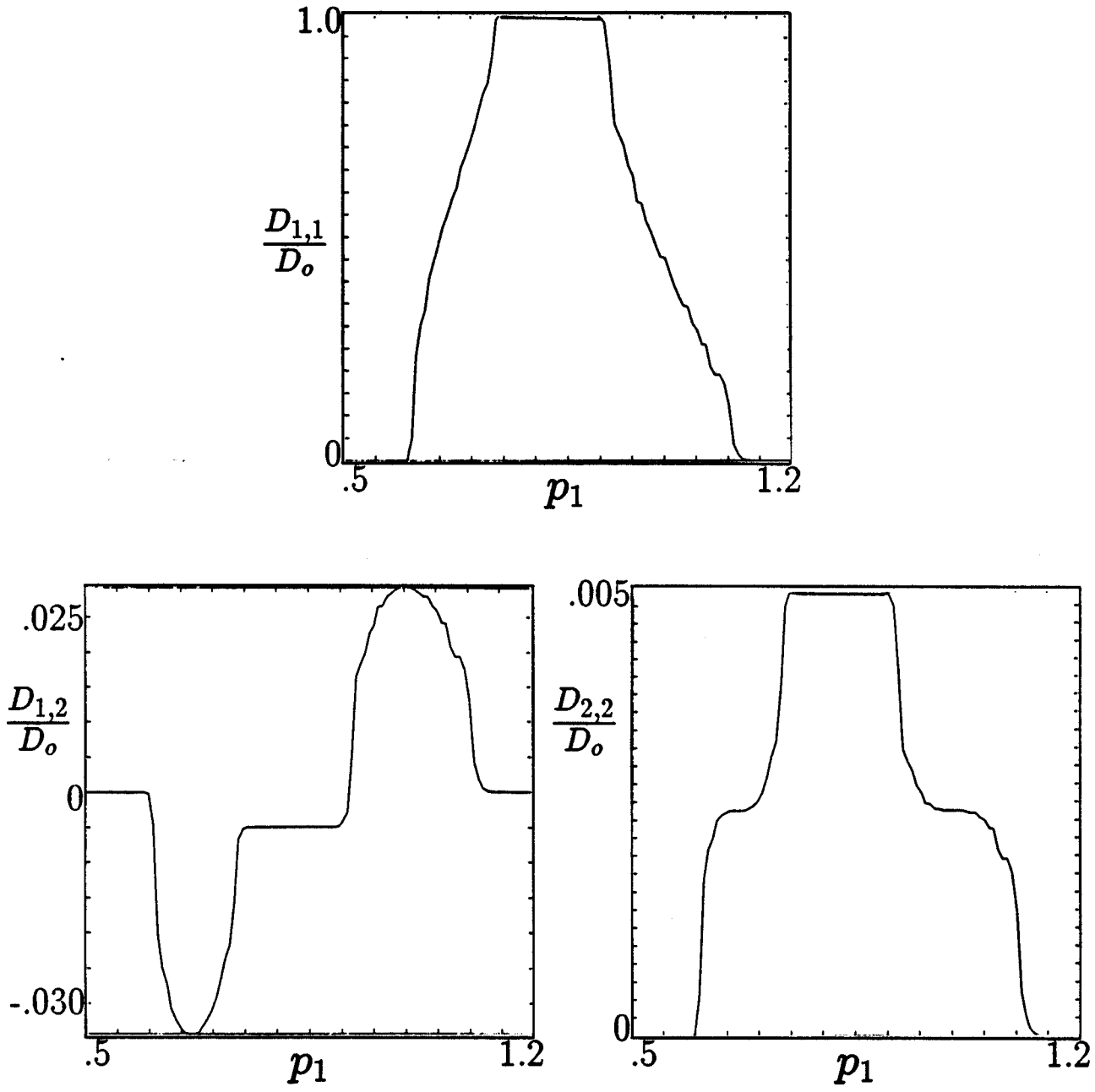

Figure 1: Elements of of quasilinear diffusion tensor, $D_{i,j}(p_1)$, determined from equation (62) for the following parameters: $n_1 = 100$, $n_2 = 150$, $q_o = 2$, $\epsilon_o = .1$, and $M = 0$. For $\epsilon_o = 0$, $D_{1,1} = D_o$ for a range of p_1 ($n_1/n_2 \leq p_1 \leq 1$) outside of which it vanishes; in this case the other elements of $D_{i,j}$ are zero for all p_1.

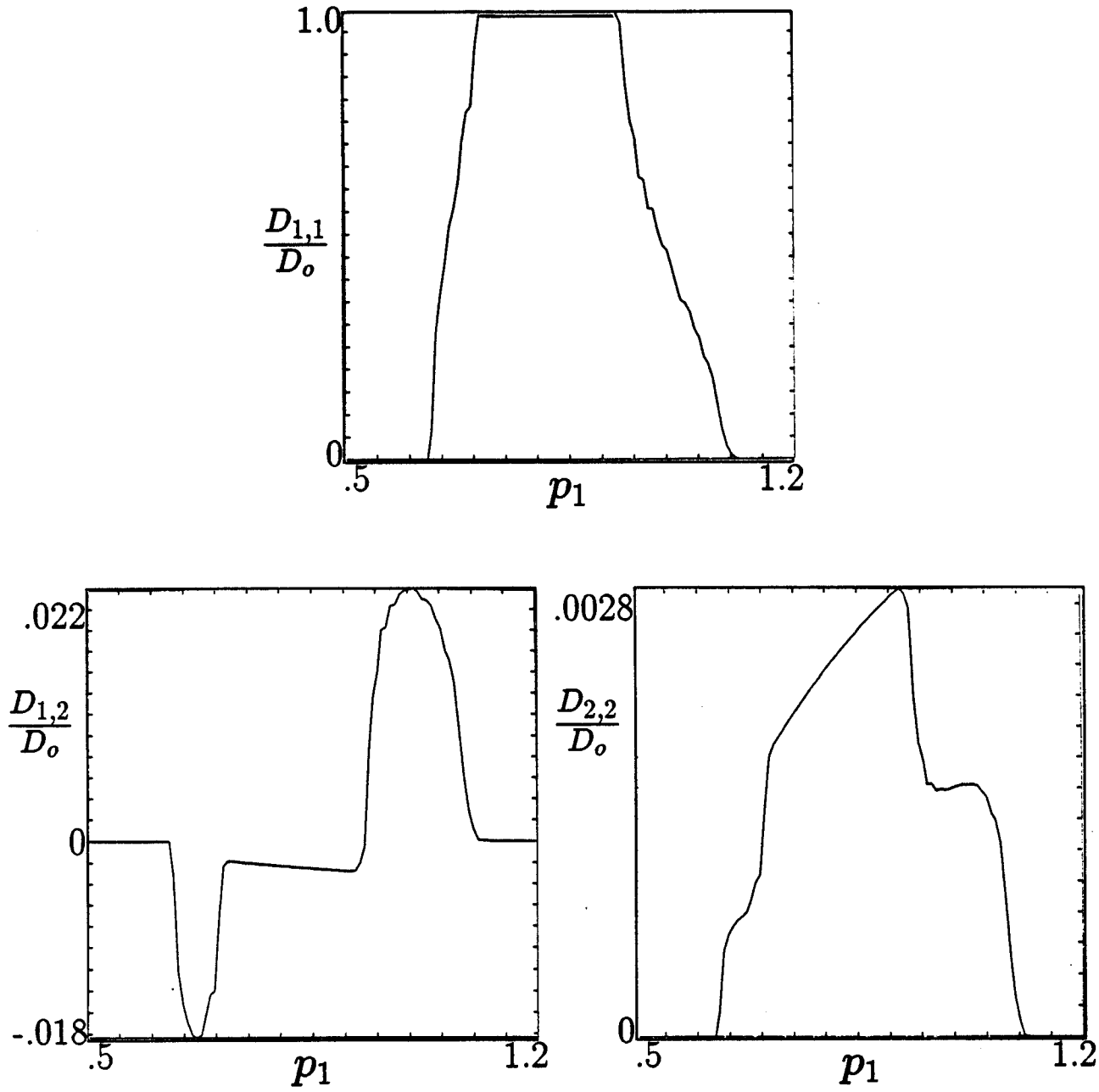

Figure 2: Elements of $D_{i,j}(p_1)$ for the same parameters as figure 1 except that $M = .2$.

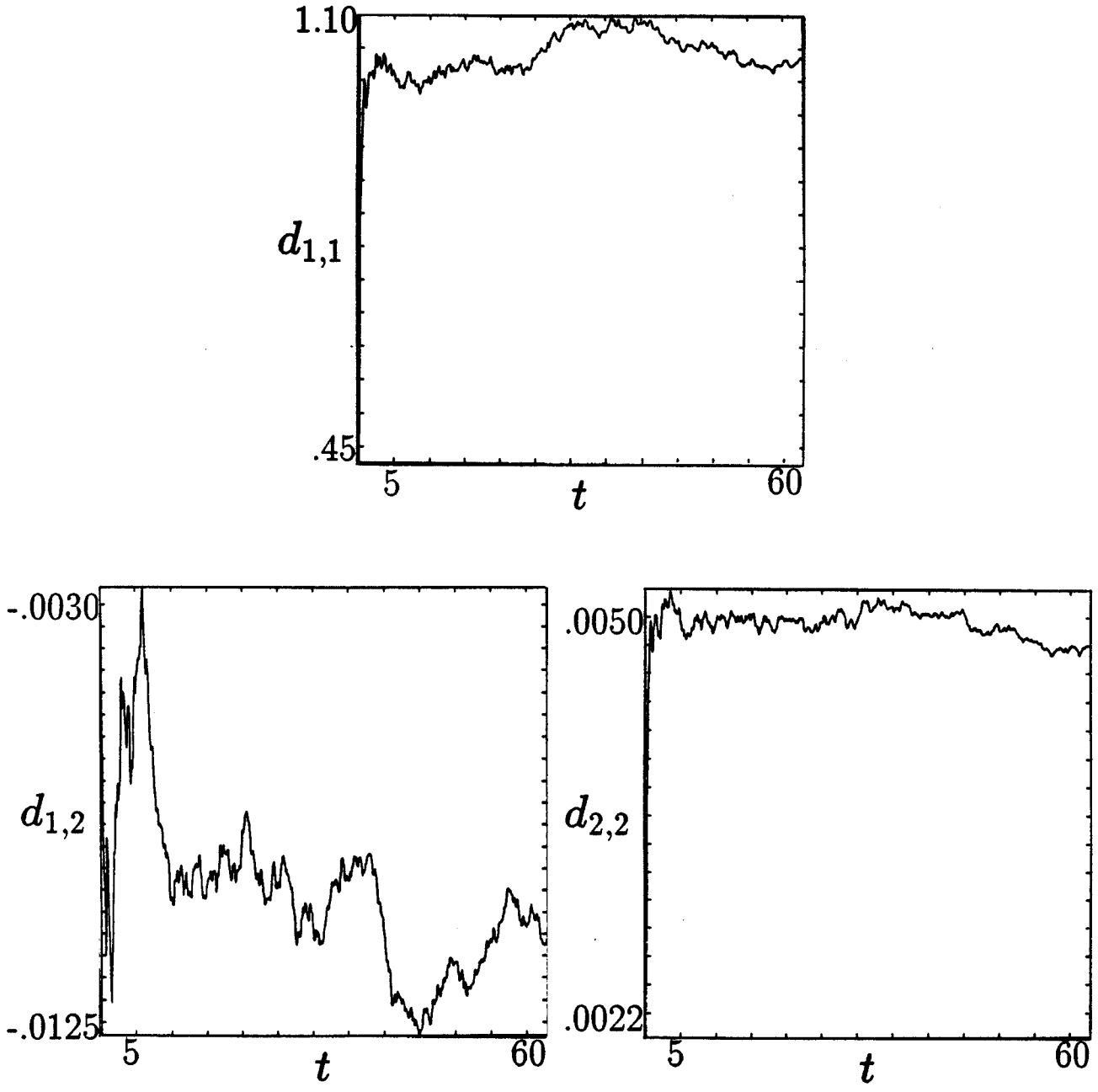

Figure 3: Elements of the diffusion diagnostic, $d_{i,j}(t; \mathbf{p}_o)$, defined in equation (63), where the parameters are the same as in figure 1 and $\Phi_o = 10^{-5}$. The ensemble of 1280 particles was initially at $p_1(0) = .8$ and $p_2(0) = 0$. (t is physical time normalized to $n_1\omega_{rf}^{-1}$).

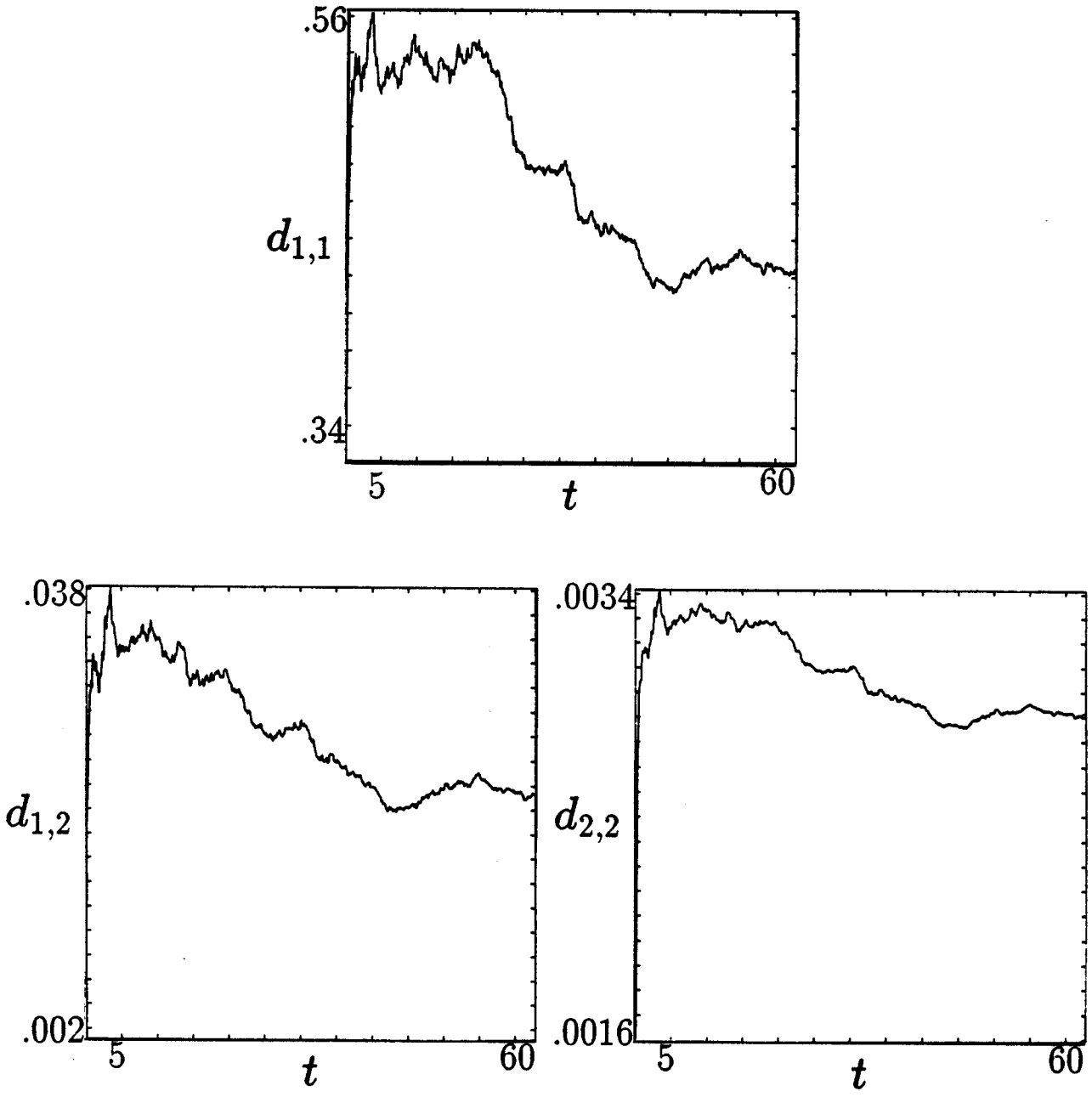

Figure 4: Elements of $d_{i,j}(t; \mathbf{p}_o)$ for the same parameters as in figure 3 except that $p_1(0) = 1.0$.

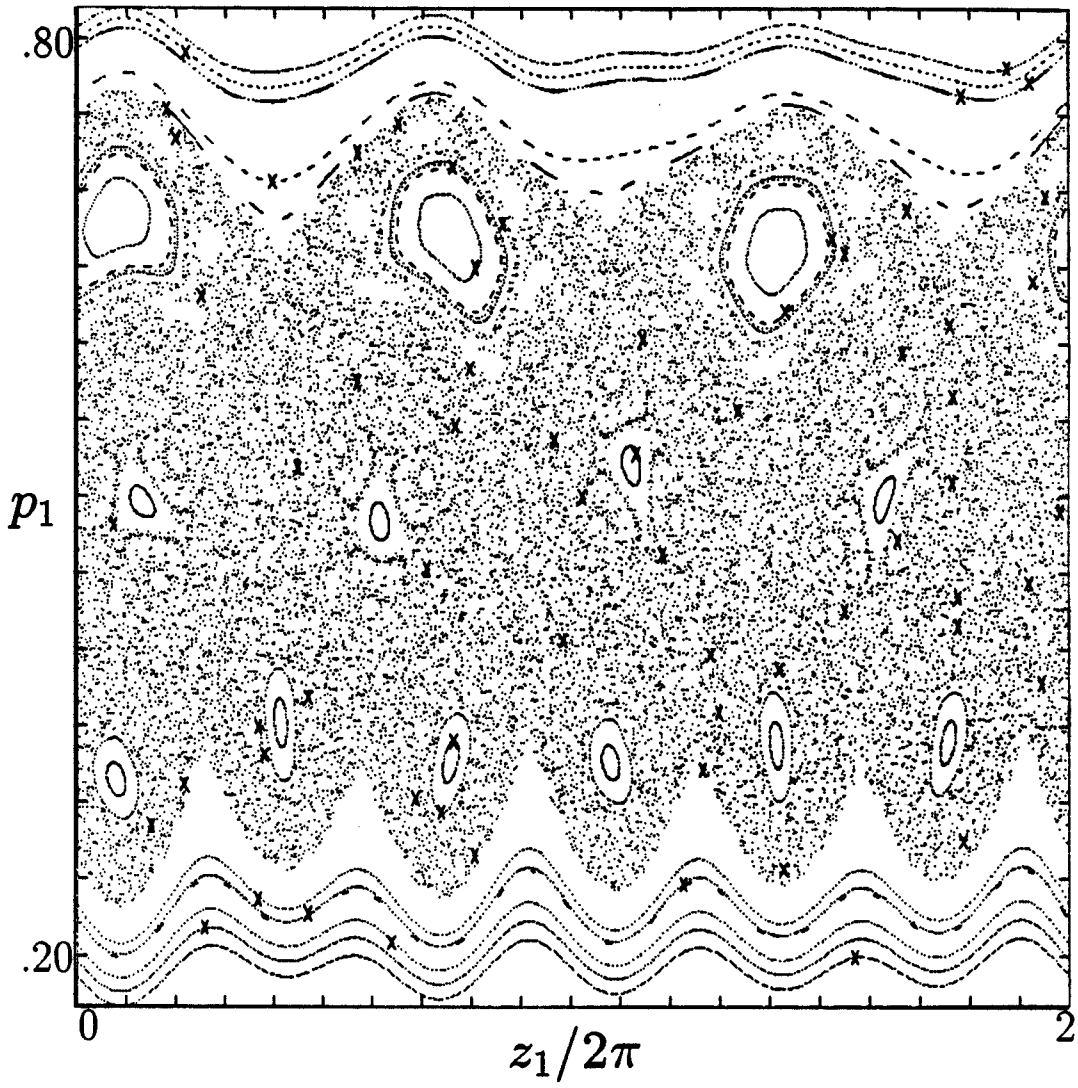

Figure 5: Surface of section, (p_1, z_1), of the parallel Hamiltonian for three waves with $\Phi_o = 2 \times 10^{-3}$, $p_2 = 0$ and $z_2 = \pi/2$. The wave-particle resonance conditions are satisfied at $p_1 = 1/3$, $1/2$, and $2/3$. Each initial condition is marked by an "X".

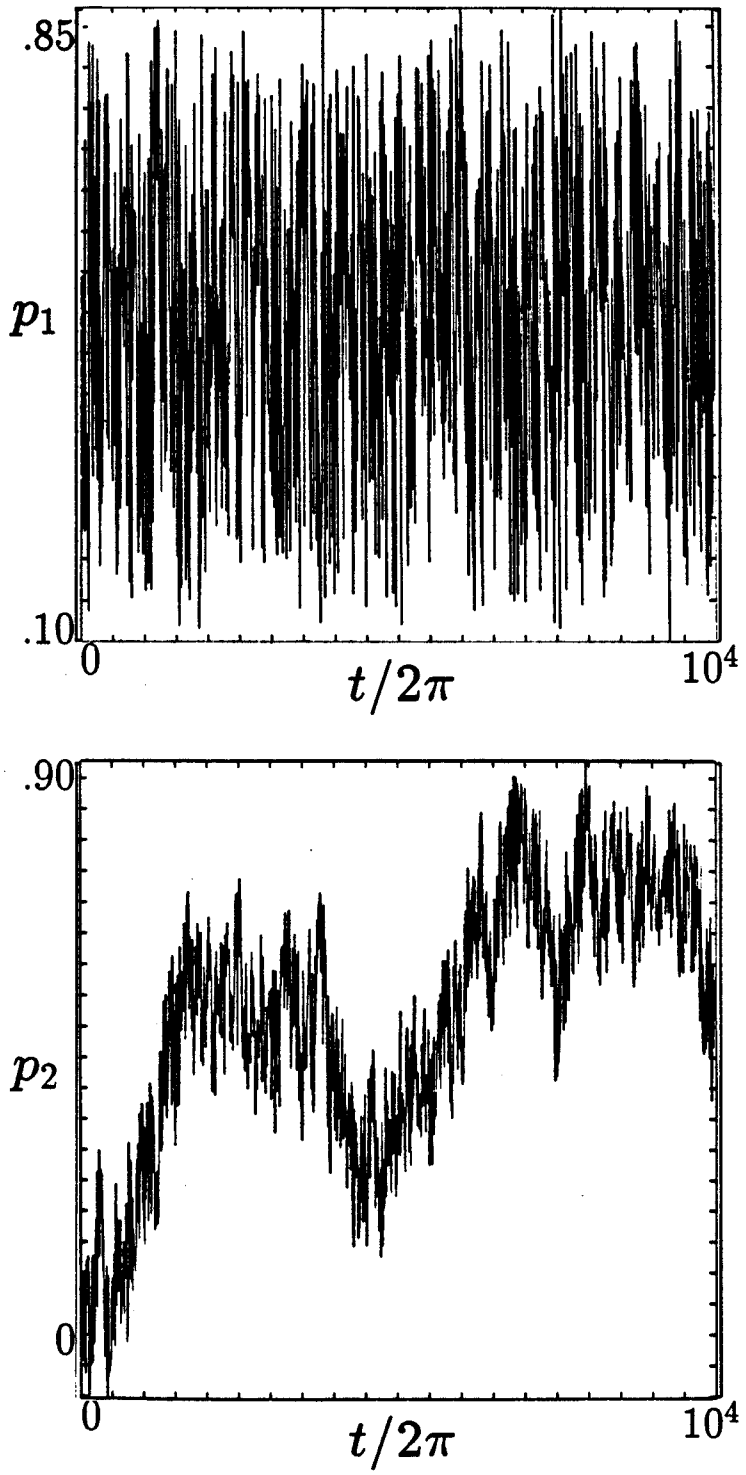

Figure 6: Stochastic time series, $p_1(t)$ and $p_2(t)$, for three waves with $\Phi_o = 10^{-2}$ and $s_o = 0$. (t is physical time normalized to ω_{rf}^{-1}).

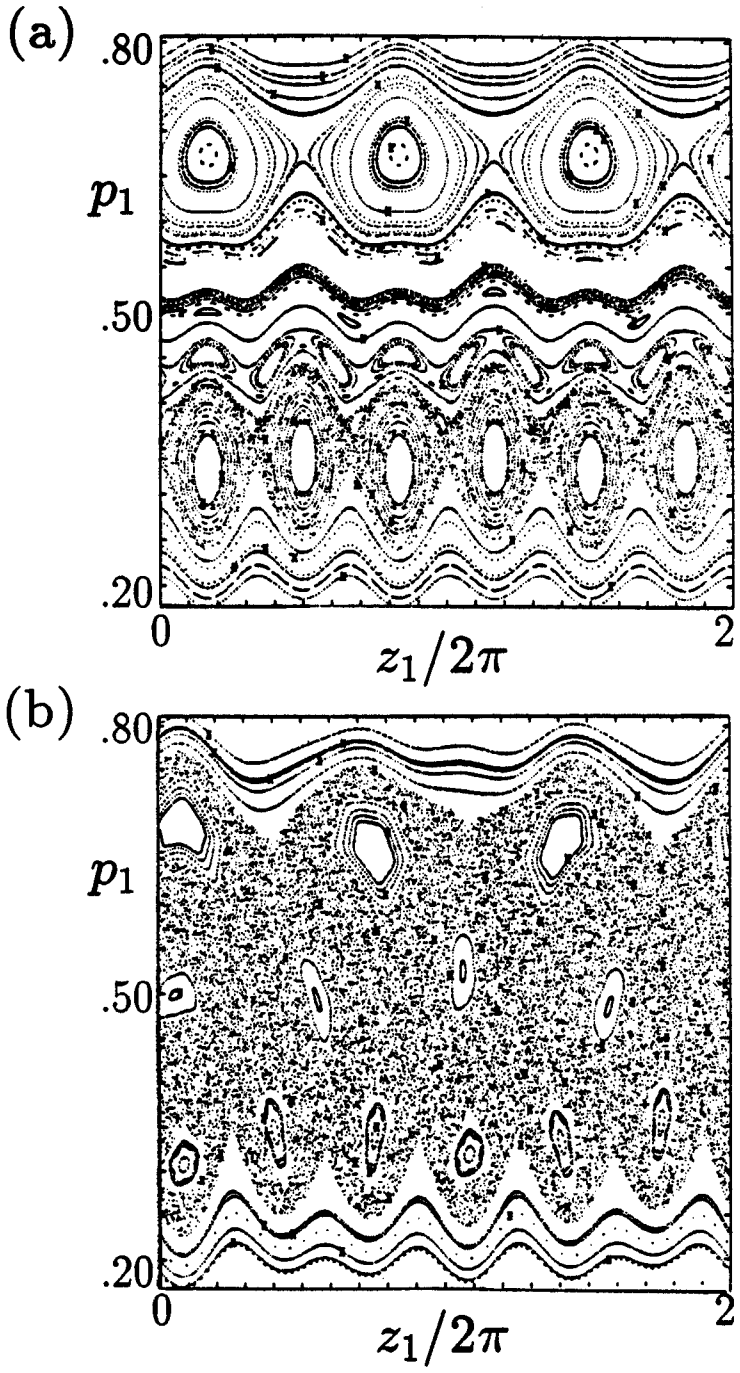

Figure 7: Surface of section, (p_1, z_1), of the parallel Hamiltonian for the four wave spectrum with degeneracy. The surface of section is shown at two values of z_2: (a) $z_2 = \pi$ and (b) $z_2 = \pi/2$, where in both cases $p_2 = 0$ and $\Phi_o = 2 \times 10^{-3}$. The wave-particle resonance conditions are satisfied at $p_1 = 1/3, 1/2$, and $2/3$, where the $p_1 = 1/2$ resonance is degenerate.

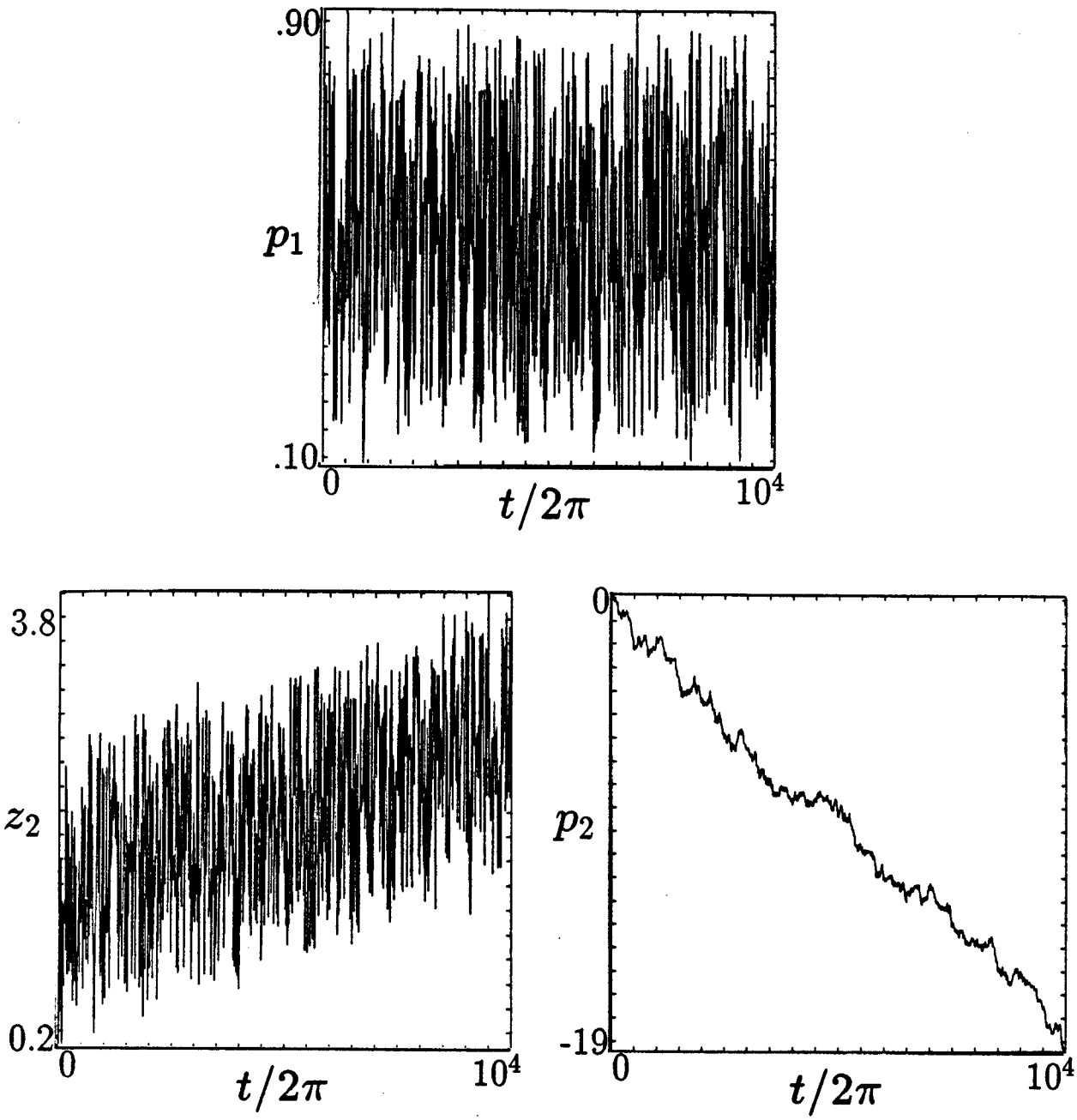

Figure 8: Stochastic time series, $p_1(t)$, $p_2(t)$, and $z_2(t)$, for four waves with $\Phi_o = 10^{-2}$ and $s_o = 0$. (t is physical time normalized to ω_{rf}^{-1}).

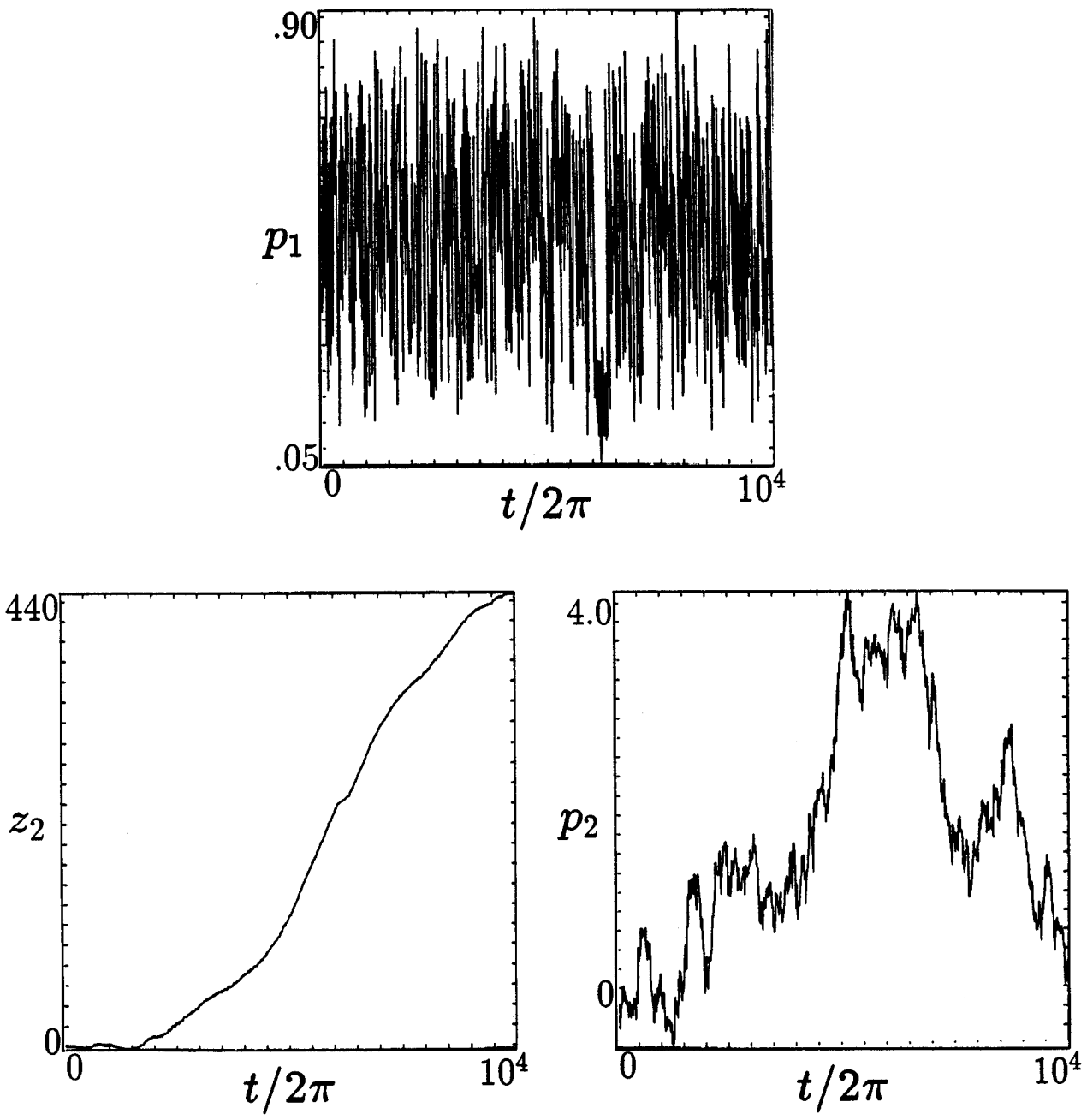

Figure 9: Stochastic time series, $p_1(t)$, $p_2(t)$, and $z_2(t)$, for four waves with $\Phi_o = 10^{-2}$ and $s_o = 10^{-2}$. (t is physical time normalized to ω_{rf}^{-1}).

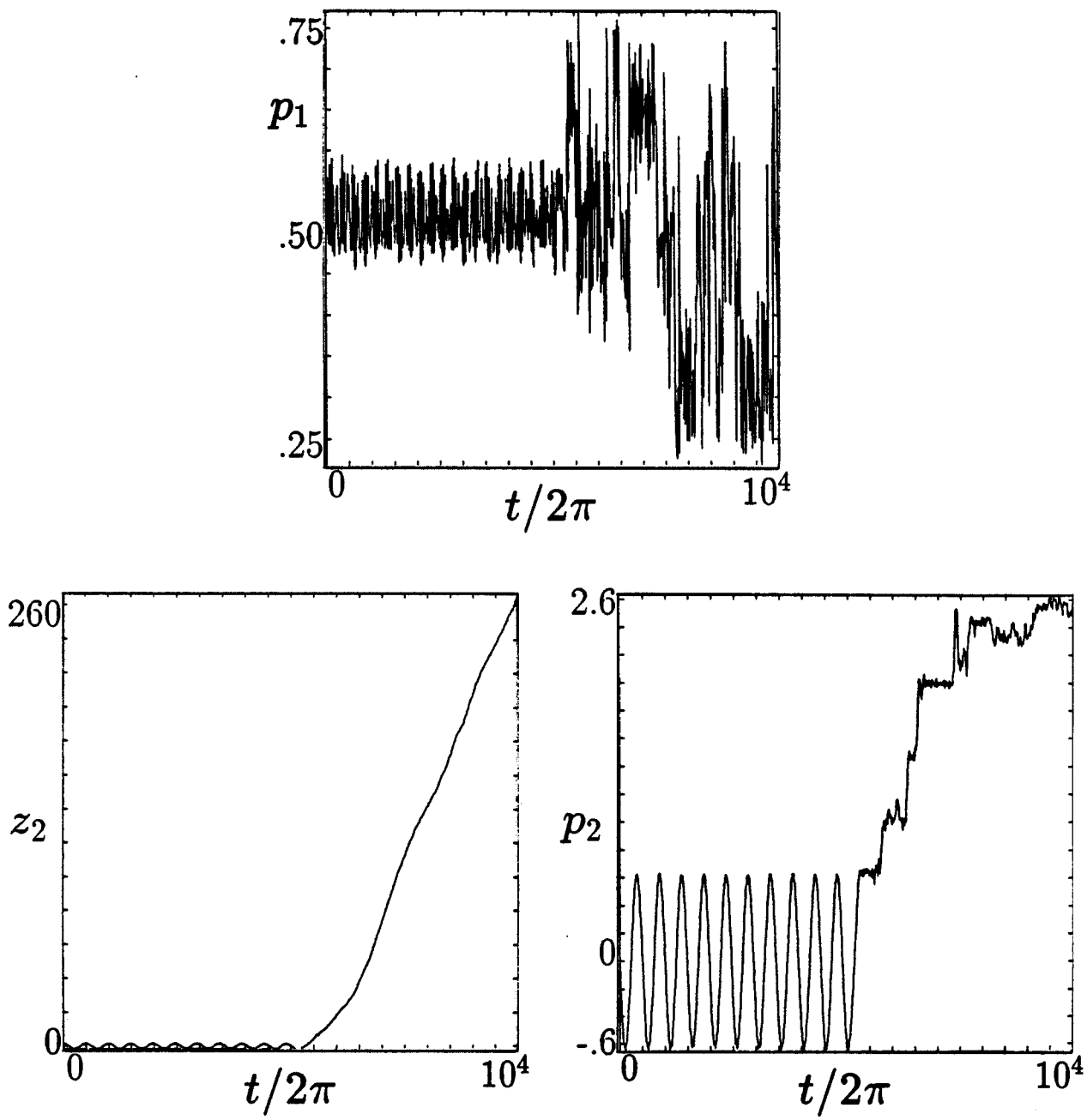

Figure 10: Time series, $p_1(t)$, $p_2(t)$, and $z_2(t)$, for initial condition in primary island of figure 7b with $s_o = 10^{-2}$. (t is physical time normalized to ω_{rf}^{-1}).

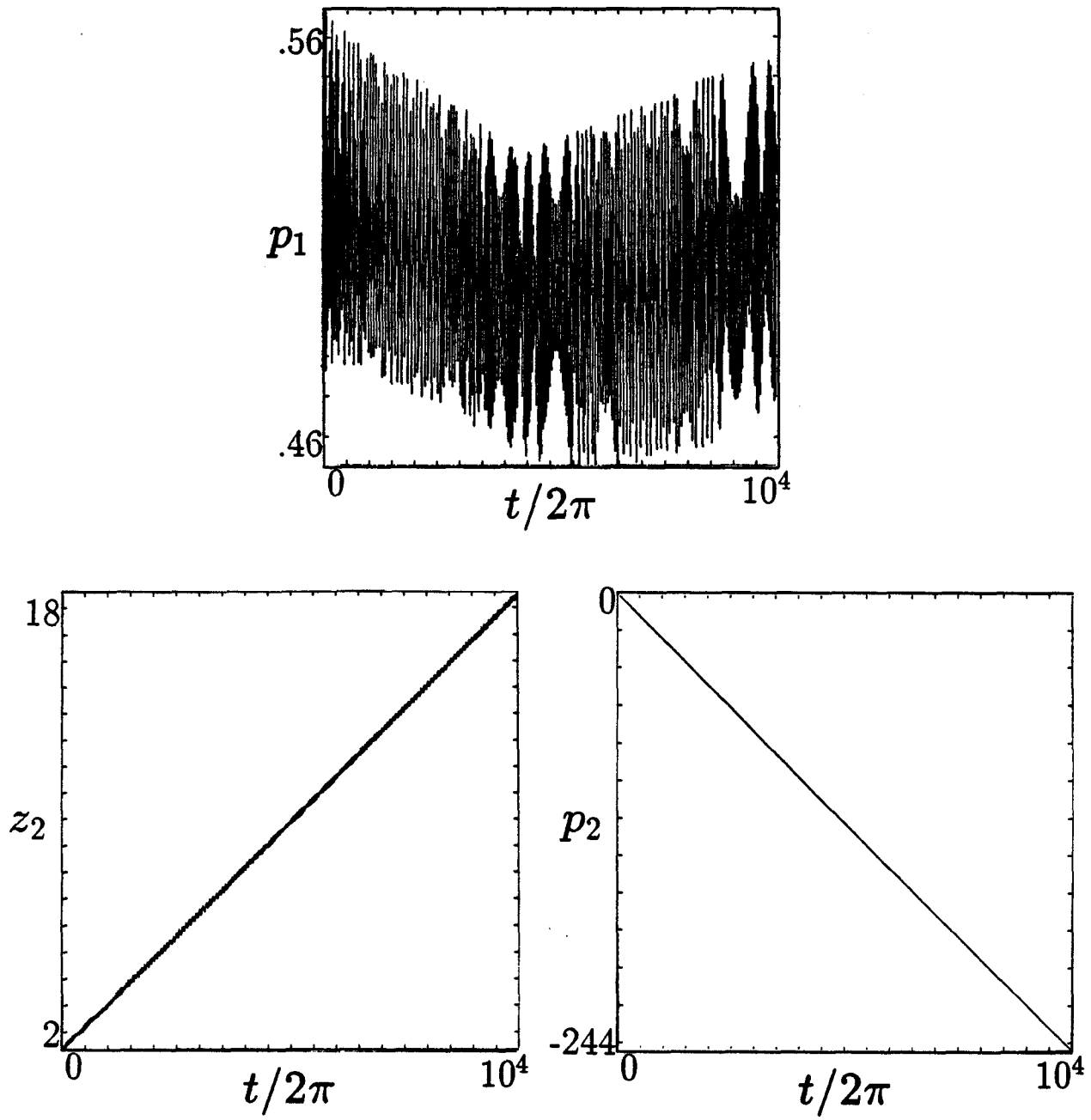

Figure 11: Time series, $p_1(t)$, $p_2(t)$, and $z_2(t)$, for initial condition in primary island of figure 7b with $s_o = 0$. (t is physical time normalized to ω_{rf}^{-1}).

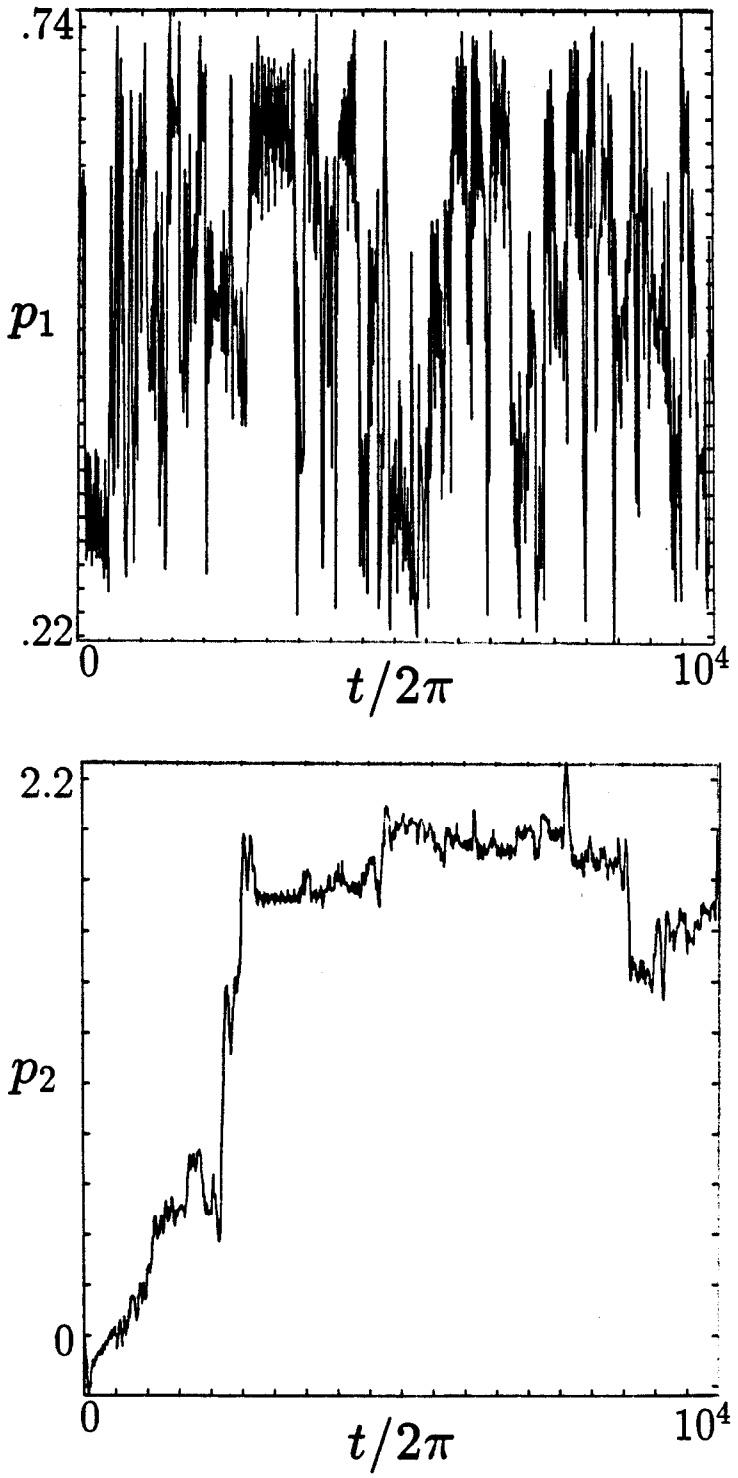

Figure 12: Stochastic time series, $p_1(t)$ and $p_2(t)$, for four waves with $\Phi_o = 2 \times 10^{-3}$ and $s_o = 10^{-2}$. (t is physical time normalized to ω_{rf}^{-1}).

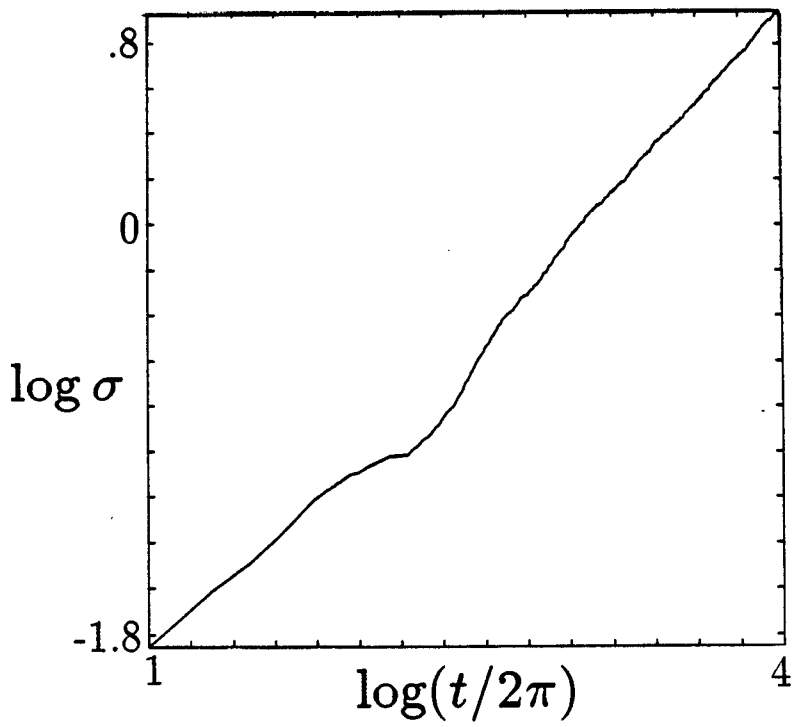

Figure 13: Log-log plot of the radial variance, $\sigma(t)$, versus time for four waves with $\Phi_o = 10^{-2}$ and $s_o = 10^{-2}$. The ensemble was orginally localized at $p_2 = 0$. (t is physical time normalized to ω_{rf}^{-1}).

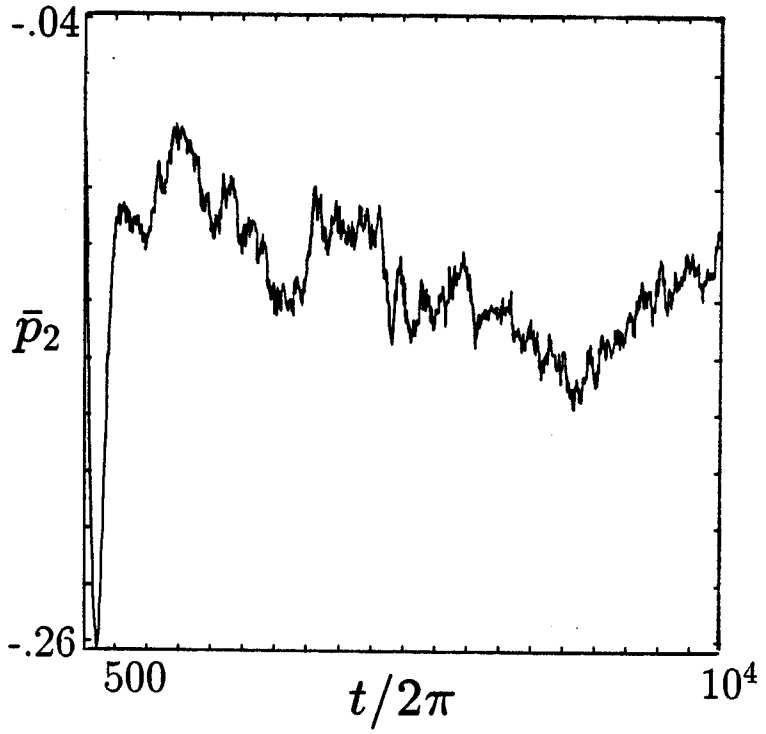

Figure 14: The ensemble average of p_2, $\bar{p}_2(t)$, versus time for the same parameters as in figure 13. (t is physical time normalized to ω_{rf}^{-1}).

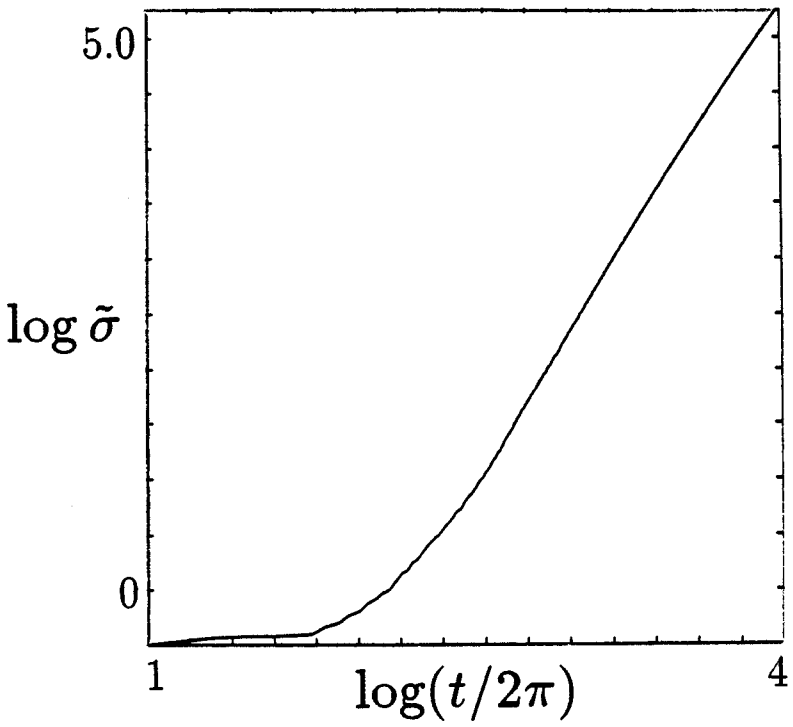

Figure 15: Log-log plot of the ensemble averaged variance in z_2, $\tilde{\sigma} \equiv \langle z_2(t)^2 \rangle - \langle z_2(t) \rangle^2$, versus time for the same parameters as in figure 13. (t is physical time normalized to ω_{rf}^{-1}).

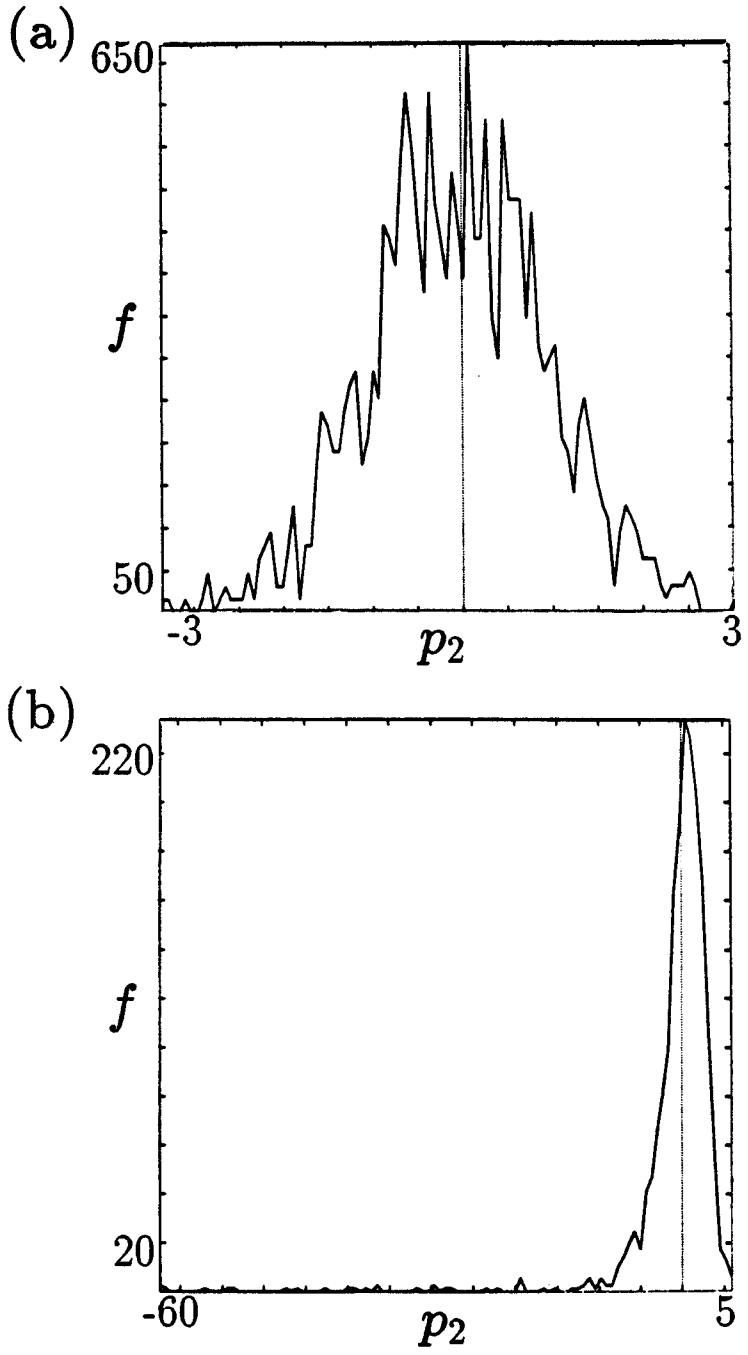

Figure 16: An ensemble of 1280 particles is initially localized at $p_2 = 0$ and spread in the stochastic region of the (p_1, z_1) plane, given by the surface of section in figure 7b. The distribution of the ensemble, $f(p_2, t)$, is shown at $t = 2\pi \times 10^4$ for two different cases: (a) $s_o = 10^{-2}$, and (b) $s_o = 0$. The dashed line marks $p_2 = 0$ and the area under each curve is equal to the total number of particles in the ensemble.